Synoptic - Dynamic Applications of Meteorological Satellite Data

Department of Meteorology
University of Wisconsin—Madison
1225 W. Dayton Street
Madison, Wisconsin 53706

Contributions by

T. H. Achtor
L. H. Horn
R. A. Marshment
D. F. Streit

L. H. Horn, Principal Investigator

FINAL REPORT

The research in this report has been supported
by the National Earth Satellite Service of the
National Oceanic and Atmospheric Administration under Grant NA 79AA-H-00011

September 1981

Synoptic - Dynamic Applications of Meteorological Satellite Data

Department of Meteorology
University of Wisconsin–Madison
1225 W. Dayton Street
Madison, Wisconsin 53706

Contributions by

T. H. Achtor

L. H. Horn

R. A. Marshment

D. F. Streit

L. H. Horn, Principal Investigator

FINAL REPORT

The research in this report has been supported
by the National Earth Satellite Service of the
National Oceanic and Atmospheric Administration under Grant NA 79AA-H-00011

September 1981

TABLE OF CONTENTS

INTRODUCTION

This report is the Final Report for research supported by the National Oceanic and Atmospheric Administration under Grant NA 79AA-H-00011. The work presented here follows naturally from our previous work which concentrated on the application of satellite indirect soundings to various synoptic and dynamic problems. A major focus of this work has involved the use of the soundings to locate the strong thermal gradients beneath upper tropospheric jets. Because the baroclinic support for jet streaks is found through a deep layer of the troposphere, the lack of vertical resolution in the satellite soundings is relatively less important than in various other applications of the sounding data.

In the first article by Streit and Horn the conditions preceding the so-called "Wichita Falls Tornado Outbreak" of 10-11 April 1979 are studied. Rather than focusing on the synoptic situation at the time of the outbreak, the study examines the events which preceded the outbreak by one to three days. The subtropical and polar jets which were of major significance to the outbreak are traced back to locations over the eastern Pacific. Both TIROS-N soundings and National Meteorological Center (NMC) analyses are used to track the locations of the jet streams. These data are used to construct both thickness fields and isentropic cross sections.

The articles by Achtor and Horn and by Marshment and Horn do not employ satellite soundings, although the implications of the studies are significant to the use of satellite soundings in tracking jet streaks and their related weather. While the satellite data can locate the jet streaks by describing their baroclinic support, these data are not capable of describing such features as the secondary circulations induced by the propagating jet. Thus Achtor and Horn have used a composite approach and conventional radiosonde data for days of Colorado cyclogenesis to relate the low level jet (LLJ) to the indirect circulation located in the exit region of the propagating jet. The presence of the LLJ, which is of importance to severe weather outbreaks has often been treated as a separate phenomena. In a second part of the study Marshment and Horn use moisture data from the days which make up the composite to describe the evolution of the moisture field and its influence on static stability during the propagation of jet streaks into the Southern Plains and the accompanying Colorado cyclogenesis.

Because satellite soundings are not capable of describing the LLJ and because they are less successful in describing moisture distributions than temperature distributions, the results of the composites obtained in these studies can form a "model" which can be used as an approximation of these phenomena in situations of propagating jet streaks and developing Colorado cyclones.

Intercomparisons of TIROS-N Satellite Sounding, Radiosonde Data and NMC Analyses in Tracking Jet Streaks

David F. Streit* and Lyle H. Horn
Department of Meteorology, University of Wisconsin-Madison

ABSTRACT

This study uses the period 8-11 April 1979 to examine the ability of TIROS-N satellite soundings to depict the evolution and eastward propagation of the polar and subtropical thermal wind jets prior to and during the Wichita Falls tornado outbreak. Both 850-300 mb thickness fields and isentropic cross sections were constructed from the satellite soundings. Unlike earlier studies, in which satellite-derived cross sections were compared with approximately coincident radiosonde cross sections, this study focuses on comparisons between TIROS-N thickness fields and cross sections oriented perpendicular to the jet streams with those obtained from National Meteorological Center (NMC) analyses. The use of NMC analyses was necessary because of the lack of radiosonde data over the Pacific Ocean, the region through which the wind maxima propagated prior to the tornado outbreak.

For one time period (0000 GMT 11 April 1979, near the time of the outbreak) radiosonde, TIROS-N and NMC cross sections were prepared. The results from this time period indicated that the TIROS-N cross section did as well as those based on NMC analyses in depicting the thermal wind maxima. This provided a certain confidence in using the TIROS-N cross sections to locate the jets over the Pacific, which is relatively lacking in conventional data. Although it was not possible to say unequivocally that the TIROS-N cross sections over the Pacific were superior to the cross sections based on NMC analyses, the results of this study suggest that they were somewhat better. This may be due in part to the fact that the thermal wind maxima were obtained from a single instrument, while the NMC analyses depended on a heterogeneous array of data.

*Present affiliation
Meteorologist, Commodity Department, E.F. Hutton & Company Inc.
One Battery Park Plaza
New York, NY 10004

1. Introduction

Considerable attention has been given to the so-called "Wichita Falls Tornado Outbreak" of 10-11 April 1979. Over forty tornadoes, hail, and strong winds were responsible for 59 deaths and 1029 injuries in this major weather related disaster. The occurrence of the outbreak during an Atmospheric Variability Experiment - Severe Environmental Storms and Mesoscale Experiments (AVE - SESAME) provided valuable supplementary data for studies of the atmospheric structure and its evolution prior to the severe weather. This study is concerned with this synoptic event, but rather than focusing on the immediate area of the outbreak, it examines the large scale pattern and its development over the period of 8-11 April 1979. The main concentration is on the upper tropospheric wind maxima using conventional radiosonde data, National Meteorological Center (NMC) analyses and vertical temperature profiles (soundings) obtained by the TIROS-N meteorological satellite.

The wind maxima present in the outbreak area on 10-11 April had propagated eastward from the Pacific Ocean and Mexico. Since these areas lack adequate radiosonde data, the use of TIROS-N soundings to define the baroclinic zone beneath the upper tropospheric wind maxima is of special interest in this study. This case provides an opportunity to examine the ability of satellite soundings to resolve these thermal gradients and their evolution over both land and ocean as they moved toward the Texas area.

One of the more successful applications of satellite soundings has been in the area of locating thermal gradients below jets (Togstad and Horn, 1974; Horn et al., 1976; Kapela and Horn, 1975; Blechman and Horn, 1981). While satellite soundings lack the vertical resolution of radiosonde soundings, the baroclinic regions below upper tropospheric jets are usually present through a deep layer. This precludes the requirement of high vertical resolution.

Within the baroclinic zone associated with the jet stream, the more intense thermal gradients are commonly associated with isotach maxima referred to as jet streaks (Palmén and Newton, 1969). These streaks propagate downwind through the larger scale jet stream located above the polar front. The transverse circulation patterns associated with jet streaks have been found to be of great importance both in cyclogenesis and also in the static destabilization of the atmosphere prior to severe storm development (Hovanec and Horn, 1975; Uccellini and Johnson, 1979; Sechrist and Whittaker, 1979; Achtor and Horn, 1981;

Marshment and Horn, 1981). On a larger scale, circulation patterns which include close proximity of the subtropical and polar jet streams (i.e., a "confluence" of the jets) are the main areas of cyclogenesis. On the other hand, severe weather outbreaks are prominent in the diffluent region where the two jets again separate (Whitney, 1977). Thus it is apparent that accurate depictions of both jet streaks and jet confluence zones are of great importance. TIROS-N soundings can help locate both of these features.

In this paper, comparisons will be made primarily between the TIROS-N and NMC analyses using both horizontal thickness fields and cross sections. The isentropic cross sections will be used to derive the thermal wind components normal to the cross section. The placement of the jet streaks will be achieved through objective analysis techniques which build the thermal wind patterns from the thermal gradients. Although data from NMC analyses will be the principal source of verification data, radiosonde sounding cross sections will also be employed for verification over the United States where radiosonde data are plentiful.

2. Data sets and procedures

Three sets of data were employed in this study to construct isentropic cross sections. The sets are satellite soundings obtained from the TIROS-N polar orbiting satellite, NMC operational analyses and raw radiosonde soundings. The latter two sets were used for verification of the satellite data.

The TIROS-N soundings were retrieved by the National Environmental Satellite Service using data from the twenty channel High-resolution Infrared Radiation Sounder (HIRS-2), the four channel Microwave Sounding Unit (MSU), and the three channel Stratospheric Sounding Unit (SSU). Since the microwave data are relatively unaffected by nonprecipitating clouds, they are useful for temperature sounding in cloudy areas. Both HIRS-2 and the MSU scan perpendicular to the orbital path over a total linear distance of 2250 km. Each HIRS-2 observation is a circular scan spot 30 km in diameter at the subsatellite point, while the MSU spot is 110 km in diameter. Through a series of procedures described in Smith et al. (1979) satellite sets containing up to seven scan spots parallel to the orbital path and nine perpendicular to it are obtained. A 7 x 9 block is used (averaged) to achieve a single TIROS-N sounding. The N-star technique described by Smith and Woolf (1976) is used in partly cloudy areas, and in cloudy

areas microwave radiances are employed. The eigenvector regression technique given by Smith and Woolf (1976) is used to obtain temperature soundings from the sets of radiance data.

The major source of verification data for testing the quality of the TIROS-N soundings was provided by NMC analyses which employ the Optimum Interpolation (OI) technique. The OI analysis was used by NMC during the First GARP Global Experiment (FGGE) year which includes the April 1979 period studied here. See McPherson et al. (1979) and Bergman (1979) regarding the NMC application of the OI analyses. The NMC data are available in gridded form at mandatory levels on a 2.5 degree latitude-longitude horizontal grid. While the NMC gridded data are based primarily on radiosonde data over the United States, they rely on a heterogeneous collection of observation systems, including buoys, aircraft, ship reports, etc. over ocean areas. It should be emphasized, however, that this collection did not include TIROS-N soundings. Over the United States, individual (raw) radiosonde soundings were also used to aid in verifying isentropic cross sections based on TIROS-N soundings and on NMC gridded data.

The use of isentropic cross sections to describe the strong thermal gradients beneath jets has a long history. See, for example, Cahir (1971) and Duquet et al. (1966). As noted in the introduction, the use of the isentropic cross section procedure to test the quality of satellite soundings in strong baroclinic zones has been pursued by our research group for several years.

In the current study, the cross sections based on TIROS-N and radiosonde (verification) data over the United States were made as coincident as possible. However, the main emphasis is on TIROS-N - NMC cross sections over the Pacific. In using NMC gridded data as verification for the TIROS-N data, the NMC data were interpolated to satellite sounding locations using a method adapted from Bleck and Haagenson (1968). (Time differences were generally less than two hours.) Consequently, it was possible to orient these cross sections in ways which provided the most information, such as locating one cross section downstream from another or placing one through the polar jet and the other through the subtropical jet. It should be kept in mind, however, that these cross sections were all done in sets of two; one based on NMC thermal data and one on TIROS-N thermal data.

An objective cross section analysis program formulated by Whittaker and Petersen (1977) was used to produce the cross sections. Isentropes and various

normal wind components are plotted on each cross section. The thermal wind relationship was used to compute the normal component of the geostrophic shear relative to 850 mb for all of the TIROS-N, NMC analyses and radiosonde normal component analyses. In addition, normal wind components using observed and "thermally enhanced" observed options of the cross section routine are included for the radiosonde data sets. The thermal enhancement technique of Whittaker and Petersen (1977) combines observed winds and thermal gradient information to enhance the wind field analysis both between stations and between the reporting levels of each station.

3. The synoptic case

The eastward propagation of both polar and subtropical wind maxima from the relatively data void Pacific and Mexican regions and their eventual interaction in the Texas area, makes this case valuable in assessing the usefulness of satellite soundings in depicting these features. The following discussion and Figs. 1 to 6 describe the major features of the circulation during the study period.

At 1200 GMT 8 April 1979, two days prior to the tornado outbreak, a well developed omega block was located over the North Atlantic at 500 mb. In contrast, there was a general zonal flow over the North Pacific as shown in the 500 mb analysis in Fig. 1. This flow had strengthened as a broad shallow trough originally east of Kamchatka drifted eastward to the Gulf of Alaska, flattening the subtropical ridge over the eastern Pacific. The mid-tropospheric zonal flow which dominated much of the central Pacific became diffluent as it approached the United States' west coast; forming a split pattern with a broad closed low centered on the southern California coast. The southern edge of this upper air low delineated the region below the subtropical jet maxima.

The 500 mb analysis at 0000 GMT 10 April (Fig. 2) reveals that in the following 36 hours a short wave trough propagated through the Pacific and deepened rapidly as it moved over the west coast of the United States and began to take on a negative tilt. An extensive surface low pressure system developed over the Rocky Mountains as the trough approached (Fig. 3). The incipient northward transport of warm air over the Great Plains, along with southward advection of cold air over the West Coast in the lower layers of the troposphere rapidly amplified the wave pattern. The closed low at 500 mb in the southwestern United

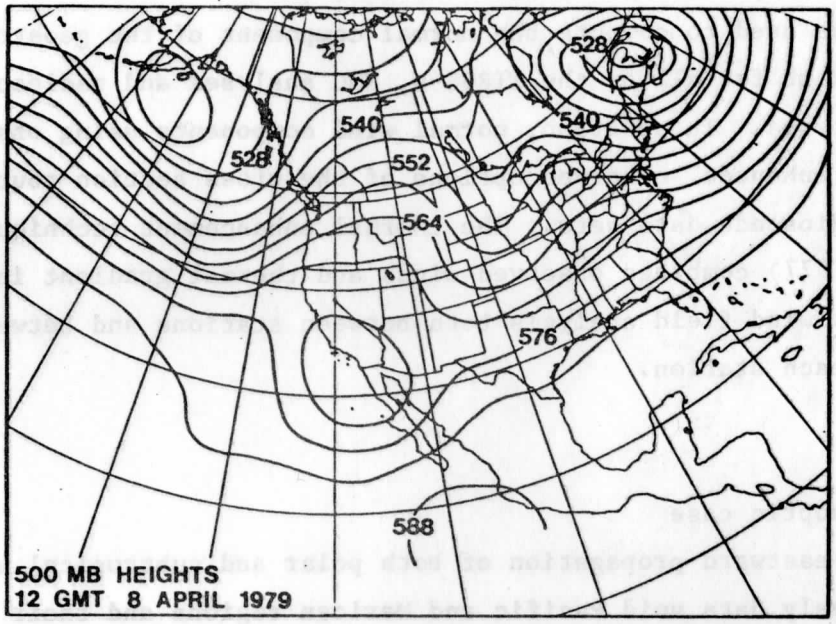

Fig. 1. 500 mb heights (dam) for 1200 GMT 8 April 1979.

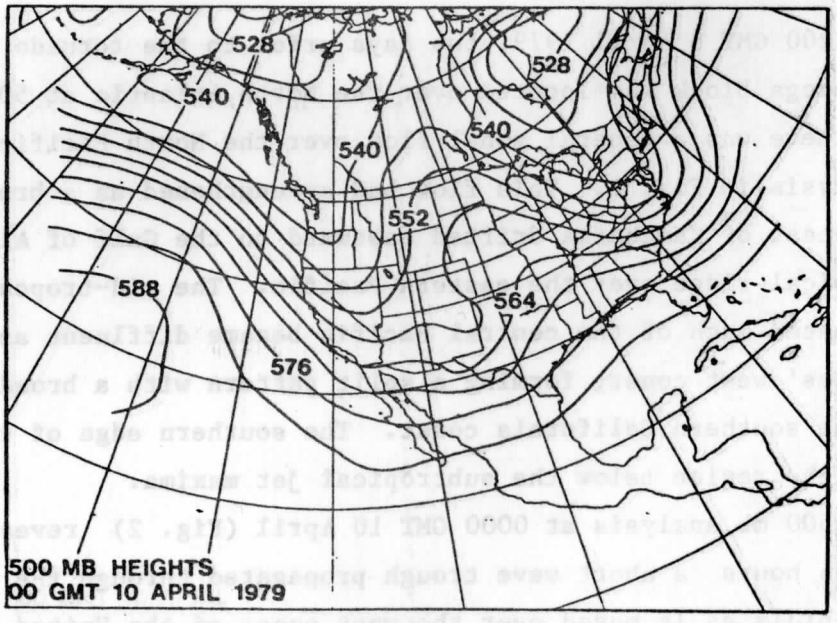

Fig. 2. 500 mb heights (dam) for 0000 GMT 10 April 1979.

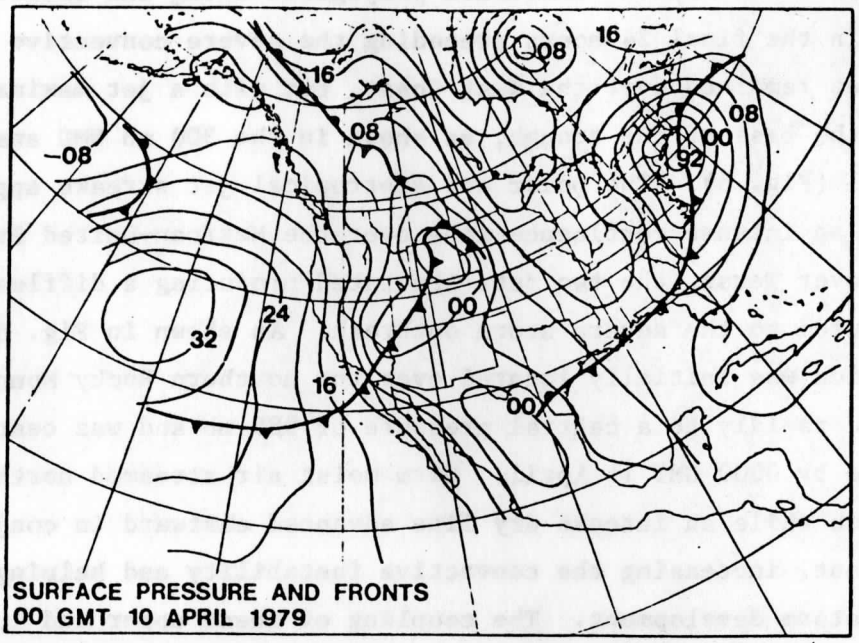

Fig. 3. Surface map (sea level pressure mb) for 0000 GMT 10 April 1979.

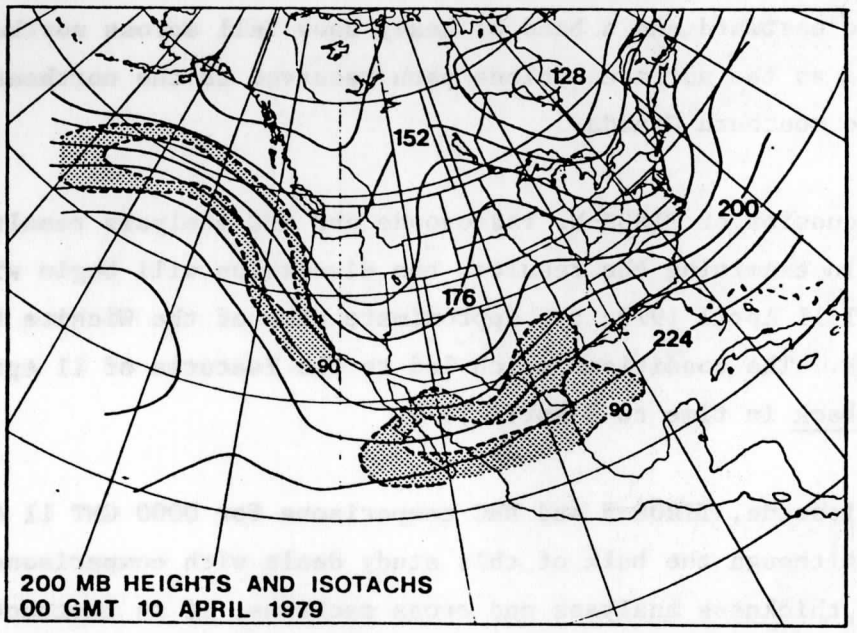

Fig. 4. 200 mb heights (dam) and isotachs (ms^{-1}) alternate intervals stipled for 0000 GMT 10 April 1979.

States in Fig. 1 opened and moved eastward over the Great Plains as a short wave in response to the approaching West Coast trough (see Fig. 2). As displayed in Fig. 4, the 200 mb NMC analysis at 0000 GMT 10 April, the polar jet streak associated with the Pacific shortwave propagated along the backside of the trough.

In the final 24 hours preceding the severe convective storm outbreak, the polar jet remained over the West Coast, but with a jet maxima propagating rapidly around the base of the trough, as shown in the 300 mb NMC analysis at 0000 GMT 11 April (Fig. 5). The polar and subtropical jet streaks approached each other to form an intense confluence zone over the Mexican-United States border. Downstream over Texas, the two jets separated producing a diffluent region which contributed to the severe storm outbreak. As shown in Fig. 6, the broad surface low, which was initially located over the northern Rocky Mountain states, deepened rapidly to a central pressure of 985 mb and was centered in eastern Colorado by 0000 GMT 11 April. Warm moist air streamed northward from the Gulf of Mexico while an intense dry line advanced eastward in conjunction with the cold front, increasing the convective instability and helping to trigger the severe storm development. The coupling of these upper and lower tropospheric features and the generation of convective instability is associated with jet streaks, as discussed by Uccellini and Johnson (1979). The strongest thunderstorms and tornadic activity was concentrated over north central Texas and southern Oklahoma. Heavy rains fell over the Southeast as the cold front advanced eastward and a band of heavy snow fell across northwest Kansas and Nebraska as the surface cyclone path recurved to the northeast through Minnesota and into southern Canada.

4. Discussion of TIROS-N, radiosonde and NMC analysis results

In examining the results, the discussion will begin with the conditions at 0000 GMT 11 April 1979, the approximate time of the Wichita Falls tornado outbreak. The conditions which led to the features of 11 April will then be traced back in time to 8 April 1979.

a. Radiosonde, TIROS-N and NMC comparisons for 0000 GMT 11 April 1979

Although the bulk of this study deals with comparisons between NMC and TIROS-N thickness analyses and cross sections, it is instructive to first briefly compare these data with nearly coincident cross sections based only on radiosonde data over the United States. These figures will not only illustrate the differences between TIROS-N and radiosonde cross sections, but also differences between cross sections based on NMC analyses and the radiosonde data.

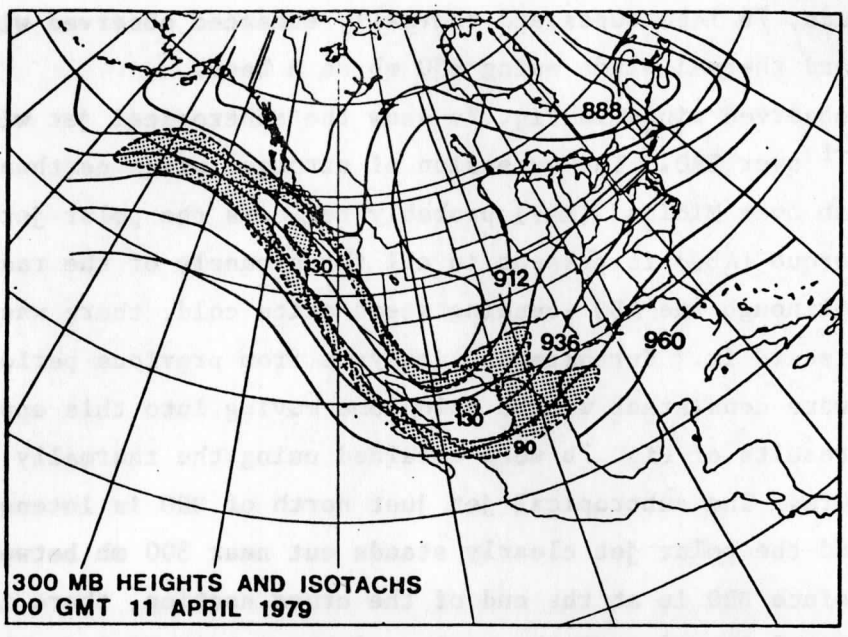

Fig. 5. 300 mb heights (dam), and isotachs (ms-1) alternate intervals stipled for 0000 GMT 11 April 1979.

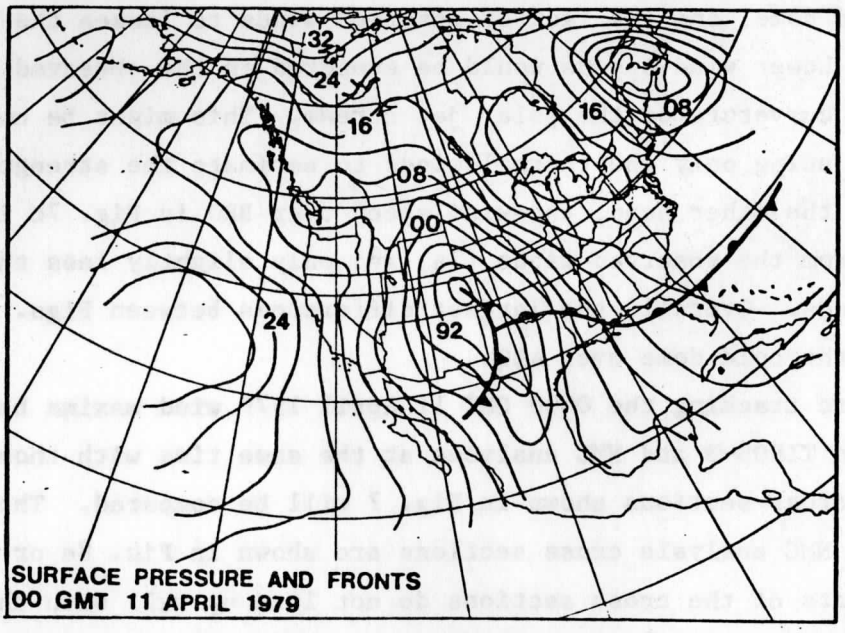

Fig. 6. Surface map (sea level pressure mb) for 0000 GMT 11 April 1979.

Fig. 7 shows radiosonde cross sections for 0000 GMT 11 April. (See Fig. 5 for the location of these radiosonde cross sections which extend southeastward from Boise (BOI) to Brownsville (BRO).) Fig. 7a shows isentropes and observed winds, 7b isentropes and thermally enhanced observed winds and 7c isentropes and thermal winds using 850 mb as a base.

The observed winds in Fig. 7a show the subtropical jet with speeds greater than 60 m s^{-1} over BRO. The extension of stronger winds northward and downward to 300-400 mb over Midland (MAF) probably reflects the polar jet. A cold dome over Albuquerque (ABQ) is present in all three panels of the radiosonde cross sections. Although the ABQ sounding seems quite cold, there was no apparent reason to discard it. Furthermore, analyses from previous periods, yet to be discussed, were consistent with a cold dome moving into this approximate area.

The results of Fig. 7b were obtained using the thermally enhanced observed wind procedure. The subtropical jet just north of BRO is intensified to over 70 m s^{-1}, and the polar jet clearly stands out near 300 mb between MAF and ABQ. (Note that since BRO is at the end of the cross section, there is some question as to the "true" location of the center of the subtropical jet.) Turning to Fig. 7c, which shows only thermal winds, the polar jet at 300 mb between ABQ and MAF is even more intense than that obtained using thermally enhanced observed winds (7b). This is due to the very large thermal gradients on the south edge of the ABQ cold dome, and the lack of observed winds to lessen the thermal wind influence. Lower wind speeds would be expected in the observed wind analysis due to cyclonic curvature of the polar jet stream. This might be considered a weakness in using only the thermal winds to estimate the strength of a jet maxima. On the other hand, the wind speed over BRO in Fig. 7c is not greatly different from the observed winds (7a) and only slightly less than the thermally enhanced winds. Overall, the largest differences between Figs. 7a, b, c seem related to the cold dome over ABQ.

Before tracking the 0000 GMT 11 April 1979 wind maxima back into the Pacific, the TIROS-N and NMC analyses at the same time with those based on the radiosonde cross sections shown in Fig. 7 will be compared. The location of the TIROS-N and NMC analysis cross sections are shown in Fig. 8a or b. Note that the northern parts of the cross sections do not line up well with the radiosonde cross sections of Fig. 7, but that through Texas, where the strongest winds were present, the radiosonde, NMC and TIROS-N cross sections are relatively coincident. Also recall that TIROS-N data were 2-3 hours earlier than the radiosonde and NMC analyses. Before comparing Figs. 7 and 8, recall from the previous synoptic discussion

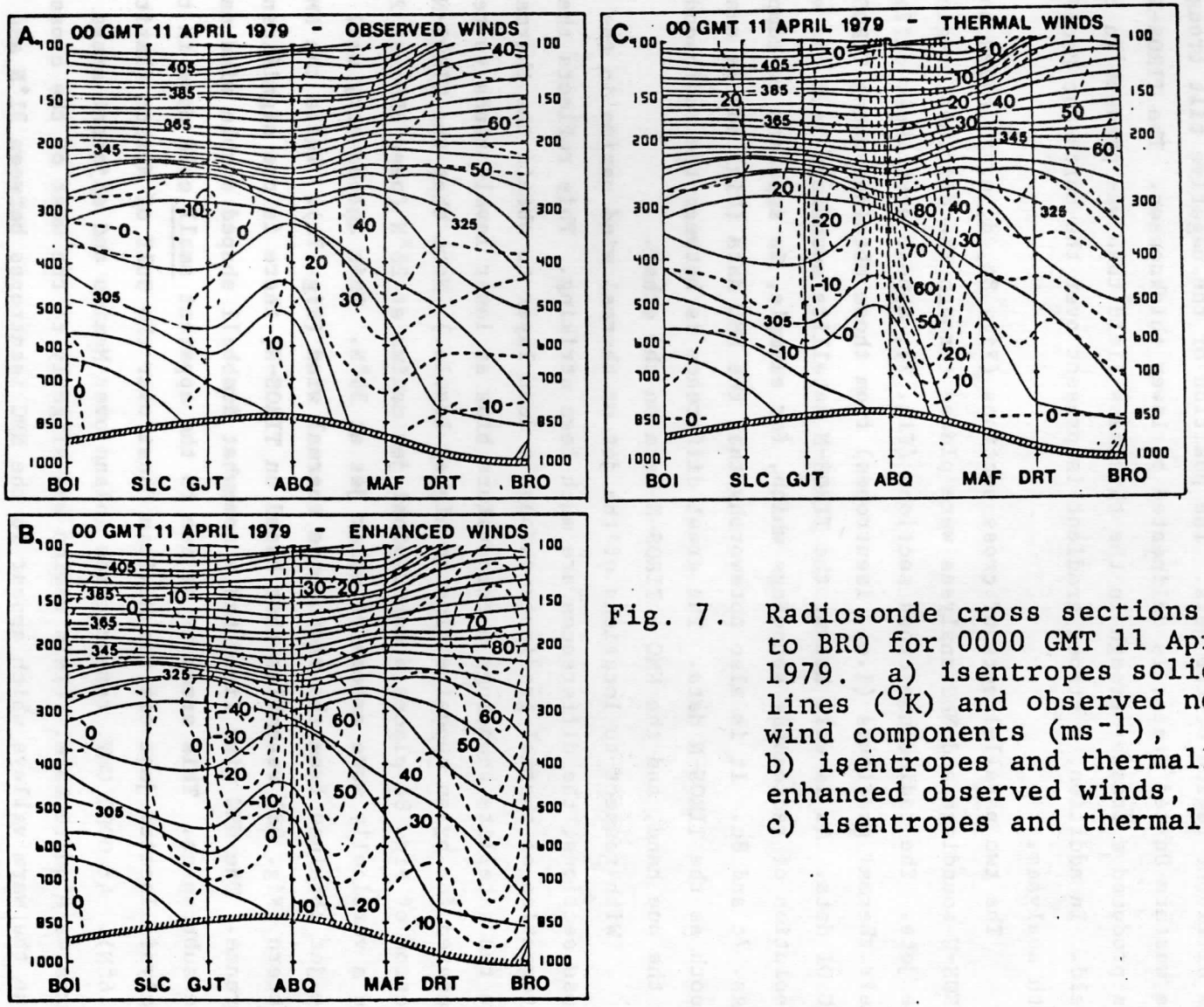

Fig. 7. Radiosonde cross sections BOI to BRO for 0000 GMT 11 April 1979. a) isentropes solid lines (^{o}K) and observed normal wind components (ms^{-1}), b) isentropes and thermally enhanced observed winds, c) isentropes and thermal winds.

that at this time the polar and subtropical jets were in close proximity over western Texas with a diffluent region downstream in the region of the tornado outbreak (see Fig. 5).

In Fig. 8a and b both TIROS-N and NMC thickness fields show spreading thickness lines (i.e., a weaker gradient) over the southern Plains, indicative of the diffluent region of the jets. The position of the negative tilt trough over the western United States is delineated by lower thicknesses. The TIROS-N analysis produced a broader trough in the thickness field than was present in the NMC field. In addition, a strong gradient is present over the northeast Pacific in both analyses.

The two parallel sets of cross sections (Fig. 8c, d, e, f) based on TIROS-N soundings and NMC analyses were placed through the diffluent region of the jets. The radiosonde cross sections (Fig. 7), appear strikingly different in their thermal gradients (i.e., isentropes) from those obtained using TIROS-N and NMC OI data. As is well known, the TIROS-N satellite soundings lack the vertical resolution of radiosonde soundings which, for example, is apparent in comparing Figs. 7c and 8c. It is also noteworthy that the NMC data (Fig. 8d) is nearly as smooth as the TIROS-N data. The great difference is between the radiosonde data on the one hand, and the NMC - TIROS-N data on the other.

With respect to locations of the jet or thermal wind maxima in the various cross sections, the differences are much less striking. This reflects the integration of thermal gradients through a deep layer to obtain the thermal wind. (In the satellite soundings a temperature bias at lower levels tends to be compensated for by an opposite bias at higher levels.) Note that the TIROS-N cross section of Fig. 8c places a subtropical jet maxima at 26°N (near BRO) at 200 mb and a vertically more extensive polar jet at 34°N. This agrees very well with the jet obtained from the radiosonde thermal wind (Fig. 7c). While the NMC wind pattern (Fig. 8d) resembles that based on TIROS-N, there is one significant difference. The NMC wind field has a somewhat dumbbell shaped double wind maxima in the subtropics. This seems to be due to the apparent small cold dome in the NMC analysis located just off the Mexican Coast over the Gulf of Mexico (latitude 23.6°N). At 0000 GMT, temperatures inland over Mexico and adjacent areas of south Texas were quite warm. (This region was slightly to the west of the cross section.) Thus the warm valleys which appear in the NMC isentropes between 31°N and 24°N may be responsible for the double wind maxima at 200 mb at 30°N and 22°N. In the three

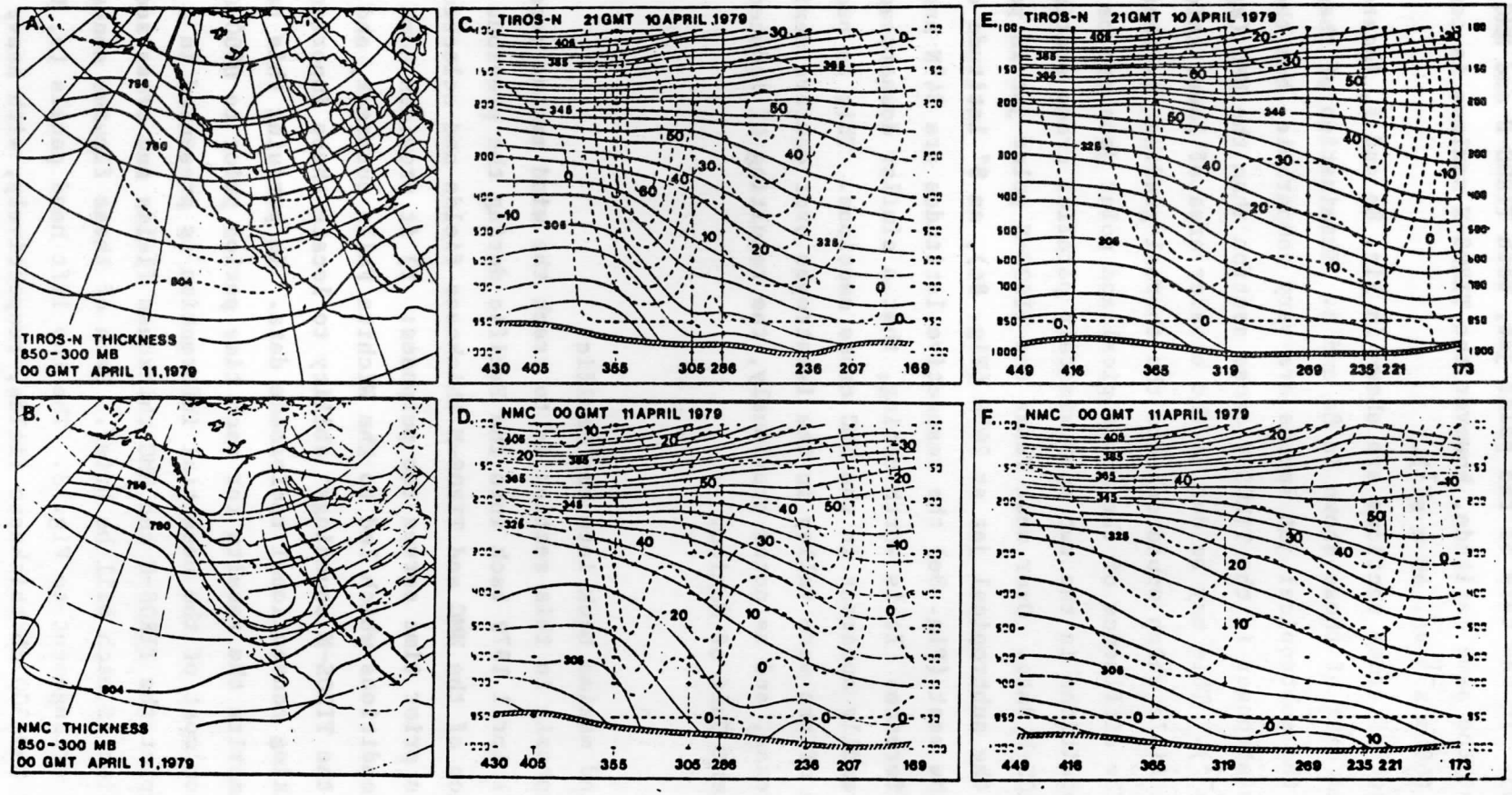

Fig. 8. Data for 0000 GMT 11 April 1979: a) Thickness field (850-300 mb) in dam based on TIROS-N data; b) same as a except NMC analysis; c) westernmost cross section of isentropes (^{o}K) and normal thermal components (ms^{-1}) based on TIROS-N data; d) same as c except using NMC analysis; e) and f) same as c and d respectively, except for eastern cross sections. Numbers at bottom of cross sections give latitudes (x 10) of sounding location, 430 = 43.0^{o}N.

dimensional analysis nature of the OI system, this warm zone is revealed. On the other hand, a single TIROS-N cross section through the area does not include this additional dimension. In the case of the polar jet, both TIROS-N and NMC place the feature at about the same latitude, however the TIROS-N maximum is considerably stronger (60 m s^{-1} vs. 40 m s^{-1}).

The second set of cross sections are shown in Fig. 8e and f, located approximately 500 km east of those shown in 8c and d. Examination of these cross sections show that the subtropical jet speeds are very comparable, but the polar thermal wind jet is stronger in the TIROS-N cross section than the NMC (again 60 m s^{-1} vs. 40 m s^{-1}). This may be due to the broader area of lower thicknesses in the TIROS-N data field which would enhance the thermal gradient farther out over the Plains. The diffluence of the subtropical and polar jets can be seen by comparing the jet positions in the two approximately parallel cross sections (Fig. 8c, e) of TIROS-N data. Over west Texas the TIROS-N polar jet is positioned at 34°N and the subtropical jet at 26°N (Fig. 8c), an 8° latitude difference, while to the east (Fig. 8e) the respective latitudes are 34°N and 23°N, an 11° latitude difference. It is worth noting, that a similar downstream separation is not readily apparent in the NMC cross sections. This is probably due to the presence of the warm valley in the isentropes over eastern Mexico and adjacent southern Texas, and as noted previously, the resulting OI induced cold dome over the adjacent Gulf of Mexico.

b. Tracking the wind maxima back into the Pacific

The major emphasis in this section is to track the wind maxima present in Texas at 0000 GMT 11 April 1979 back into the Pacific during the previous three days. An examination of the NMC and TIROS-N thickness fields and selected cross sections during this prior time serves two purposes: 1) it provides some insight into the synoptic conditions which led to the Wichita Falls outbreak, and 2) it provides a test of the TIROS-N soundings' ability to locate these important wind maxima in areas lacking conventional radiosonde data. In pursuing this task, the discussion will summarize the results for each time period prior to 0000 GMT 11 April 1979. Since most of the essential information is presented in a series of figures which depict the TIROS-N and NMC thickness fields and cross sections, the written discussion of each will be brief. Each of these figures contain six panels in a similar arrangement to Fig. 8. The two left hand panels (a, b) show the TIROS-N and NMC 850-300 mb thickness fields, respectively, with heavy dashed

lines indicating the location of cross sections displayed in panels c and e for TIROS-N and d and f for NMC data.

1) 1200 GMT 10 April 1979

Figure 9 displays the thickness fields and cross sections about twelve hours prior to the outbreak of severe weather. A strong thermal gradient exists over the northeast Pacific with lower thicknesses extending southward across the western United States. These characteristics are similar to those at the time of the tornado outbreak. The greatest discrepancy between the NMC and TIROS-N fields is over the Pacific west of Mexico, where the thickness gradient is more zonally oriented and slightly stronger in the TIROS-N analysis. This arrangement suggests more thermal support for the polar jet near the coast of the United States in the NMC data, but slightly more thermal support for the subtropical jet to the south and west over the Pacific in the TIROS-N data. The tighter packing in the NMC analysis may be due to the greater amount of radiosonde data along the west coast of the United States.

As done previously, two parallel cross sections were constructed, extending from the western United States southward across the Pacific west of the Mexican coast, to compare the polar and subtropical jets simultaneously. Relatively large fluctuations of the upper tropospheric isentropic field off the west coast in the westernmost NMC cross section (Fig. 9d) result in significant differences in the thermal wind field compared to TIROS-N (Fig. 9c). Both jets are stronger in the NMC OI cross section than TIROS-N and show an unrealistic easterly wind component near 300 mb between the jets, which does not appear in the TIROS-N analysis. It should be noted that the NMC 300 mb chart for 1200 GMT 10 April failed to show any easterly flow in this region. Since 300 mb winds include aircraft reports, it appears that in this area the TIROS-N results may be more realistic than the NMC OI thermal wind fields. Both jet cores are displaced 3-4° latitude to the south in the NMC cross sections compared with TIROS-N. The comparable TIROS-N and NMC wind speeds north of the jet core over the western United States, where radiosonde data are present, further support the TIROS-N locations of the jet core.

The discrepancy in the thickness fields off the Mexican coast shows up in Fig. 9e and f, where the NMC thermal wind field fails to depict the subtropical jet. (Note, only one wind maxima is present in Fig. 9f.) On the other hand, in the TIROS-N data the subtropical and polar jets approach each other over the Mexican coast, but still have separate thermal wind maxima in the general region that the NMC data shows a stronger single jet.

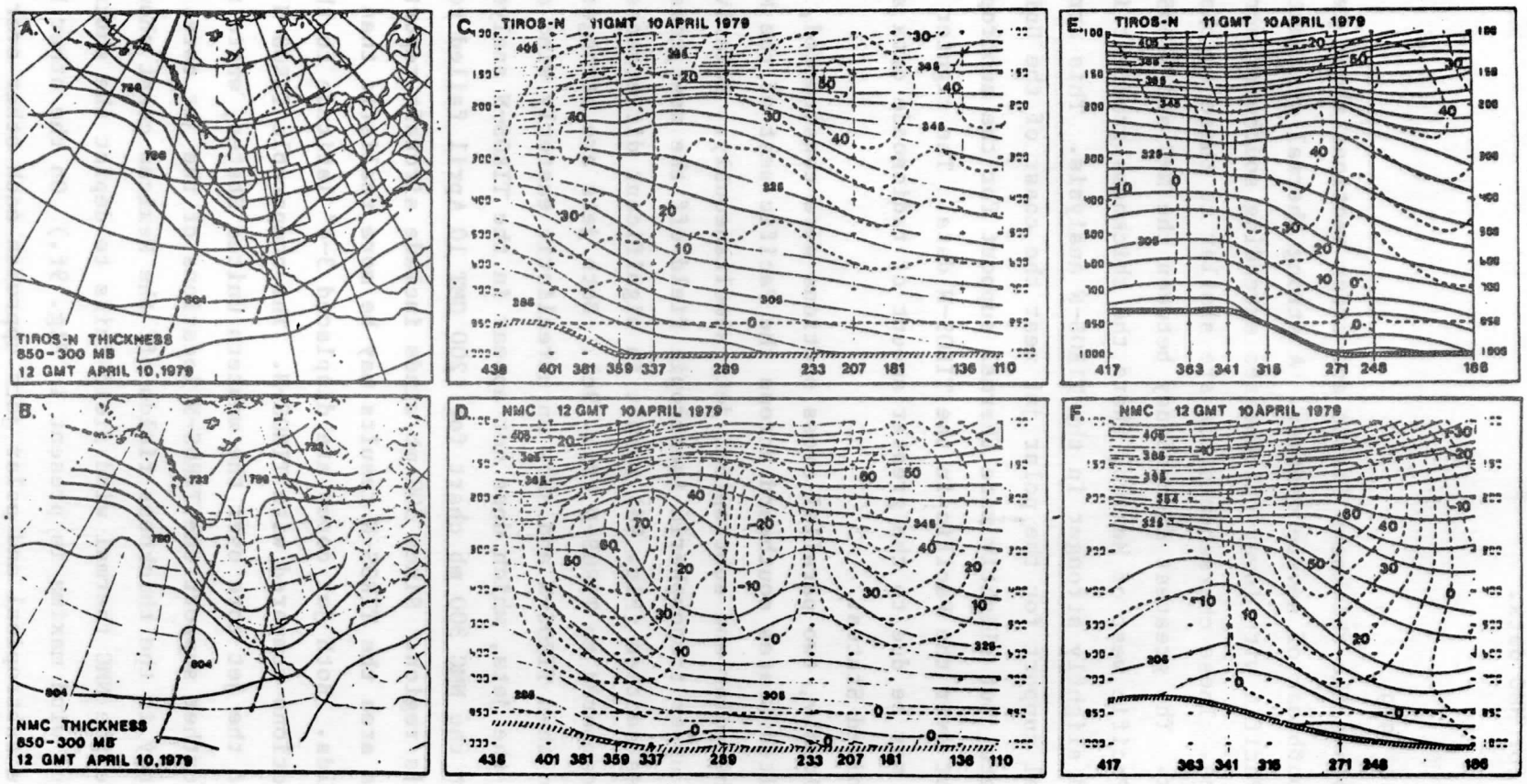

Fig. 9. Data format same as Fig. 8 except for 1200 GMT 10 April 1979.

2) 0000 GMT 10 April 1979

Fig. 10 shows that good agreement between the NMC and TIROS-N thickness fields is present everywhere, most notably over the south central United States. In this area, the extension of lower thicknesses from the southern Rockies eastward over the Plains is reflected in both analyses (Fig. 10a and b). In choosing cross sections for 0000 GMT 10 April, it was not possible to construct a cross section west of the westernmost cross section shown in the previous figure because a data gap existed between TIROS-N orbits over this area. Consequently, the two cross sections shown in Fig. 10 a and b were chosen. There was some advantage to this, in that the westernmost TIROS-N cross section (Fig. 10c) stays in a location approximately midway between Fig. 9c and e off the coast of Mexico. This permits the depiction of the polar jet nose propagating into this region. The western cross section, running from Arizona southwestward over the Pacific, is shown in Fig. 10c and d. A low level cold dome over the relatively cooler water of the Pacific evidently has a much greater effect on the NMC thermal wind field than on the TIROS-N thermal wind field. The TIROS-N cross section more realistically delineates the strong subtropical jet maxima over the ocean (near 20°N) and the nose of the polar jet just beginning to push southward just west of Baja, California (at about 27°N). It is somewhat disconcerting that the polar jet has a relatively high elevation compared with the subtropical jet. There is no readily apparent explanation except that only the nose of the jet appears. It is common for the polar jet core to descend as it propagates around the wave. In contrast, the NMC cross section (Fig. 10d) fails to capture this double wind maxima, showing a broad zone of stronger winds extending from about 29°N to 23°N. This is evidently due once again to exaggerated low level effects (i.e., the cold dome near 28°N) on the upper tropospheric wind field. Subsequent analyses (1200 GMT 10 April and 0000 GMT 11 April) appear to have confirmed the TIROS-N interpretation over that given in the NMC cross sections.

To investigate the cold trough that extended eastward over the southwestern Plains, the eastern cross section was constructed perpendicular to the trough in the thickness pattern. In Fig. 10e and f, both isentropic fields show the cold dome structure as expected, in the area of lower thicknesses (and in general agreement with the ABQ cold dome noted earlier in Fig. 7). Another weak cold dome appears in both cross sections over the Gulf of Mexico possibly due to the relatively cooler sea surface temperatures during the day. In these cross sections, the thermal wind fields similarly show a strong thermal wind jet located near 33°N over Texas. This jet maxima reflects the intensified thermal gradient associated with the short wave

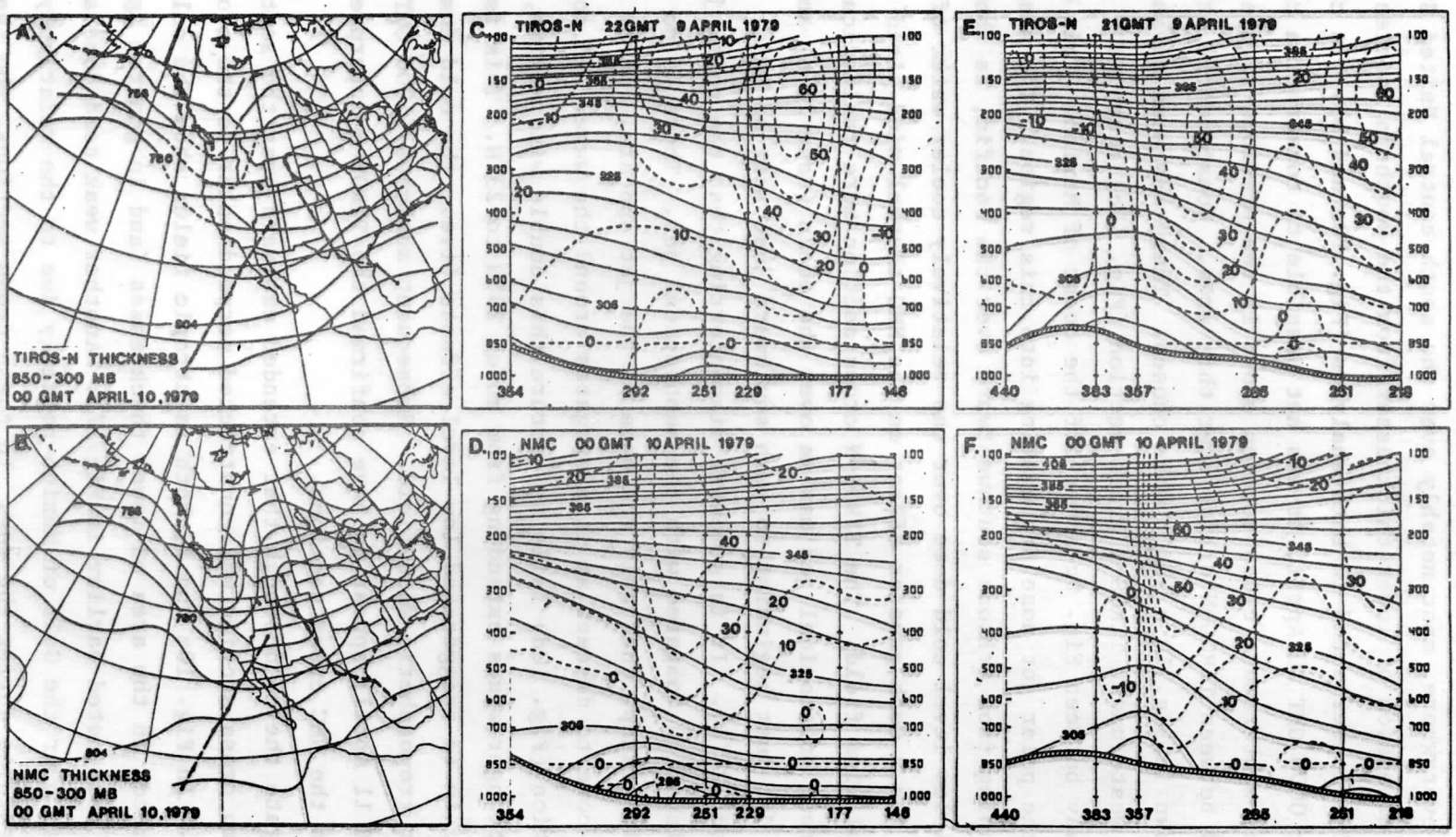

Fig. 10. Data format same as Fig. 8 except for 0000 GMT 10 April 1979.

that propagated out over the Plains at 0000 GMT 10 April as described in the synoptic section. The second jet maxima (i.e., the subtropical jet) over the Gulf is positioned near 22°N in both cross sections, but is much stronger in the TIROS-N analysis (60 m s^{-1} vs. 30 m s^{-1}). A factor that may have caused the smaller wind speeds found in both cross sections in the region between the two wind maxima is that the angle of the cross sections in this area departs from normal to the thickness lines which decreases the gradient.

3) 1200 GMT 9 April 1979

Twelve hours earlier, the lower thicknesses are much farther north in the western United States reflecting the rapid development between 1200 GMT 9 April and 0000 GMT 10 April. There is one major disagreement between thickness fields located over the northeast Pacific (see Fig. 11). The NMC thermal gradient is noticeably stronger than the TIROS-N gradient over the ocean area. This difference is even more apparent in the westernmost cross section (Fig. 11c and d), which runs from the southeastern Alaskan coast south-southwest to about 20°N. In this cross section, the TIROS-N thermal wind field denotes a much weaker polar jet maxima (30 vs. 50 m s^{-1}) than the NMC data, even though the location of the jet core is comparable. At this point it is difficult to state conclusively which analysis is more accurate.

Briefly turning to the eastern cross section at 1200 GMT 9 April (Fig. 11e and f), very good agreement is noted between the NMC and TIROS-N cross sections. Both place a polar jet at about 42°N and 250 mb (40 m s^{-1} maximum wind speeds for TIROS-N and 50 m s^{-1} for NMC data). The subtropical jet is near the southern end of the cross section at about 21°N. While it appears in both data sets, it is somewhat stronger in the TIROS-N data. It is these two jets, located well out over the Pacific at 1200 GMT 9 April, that eventually played an important role two days later in the Wichita Falls outbreak.

A troubling factor remains concerning the discrepancy between the TIROS-N and NMC western cross section (Figs. 11c and d). In regions of inadequate radiosonde data, it is difficult to rely strongly on NMC thermal gradients. In dealing with actual winds, the NMC data include aircraft reported winds, etc., but recall that in this study the concern is over thermal gradients. The <u>isotach</u> analysis on the 1200 GMT 300 mb NMC chart suggests <u>actual</u> wind speeds of about 40-45 m s^{-1} at the location of the wind maxima displayed in the cross sections. This compares with a thermal wind speed of about 30 m s^{-1} at 300 mb in TIROS-N and

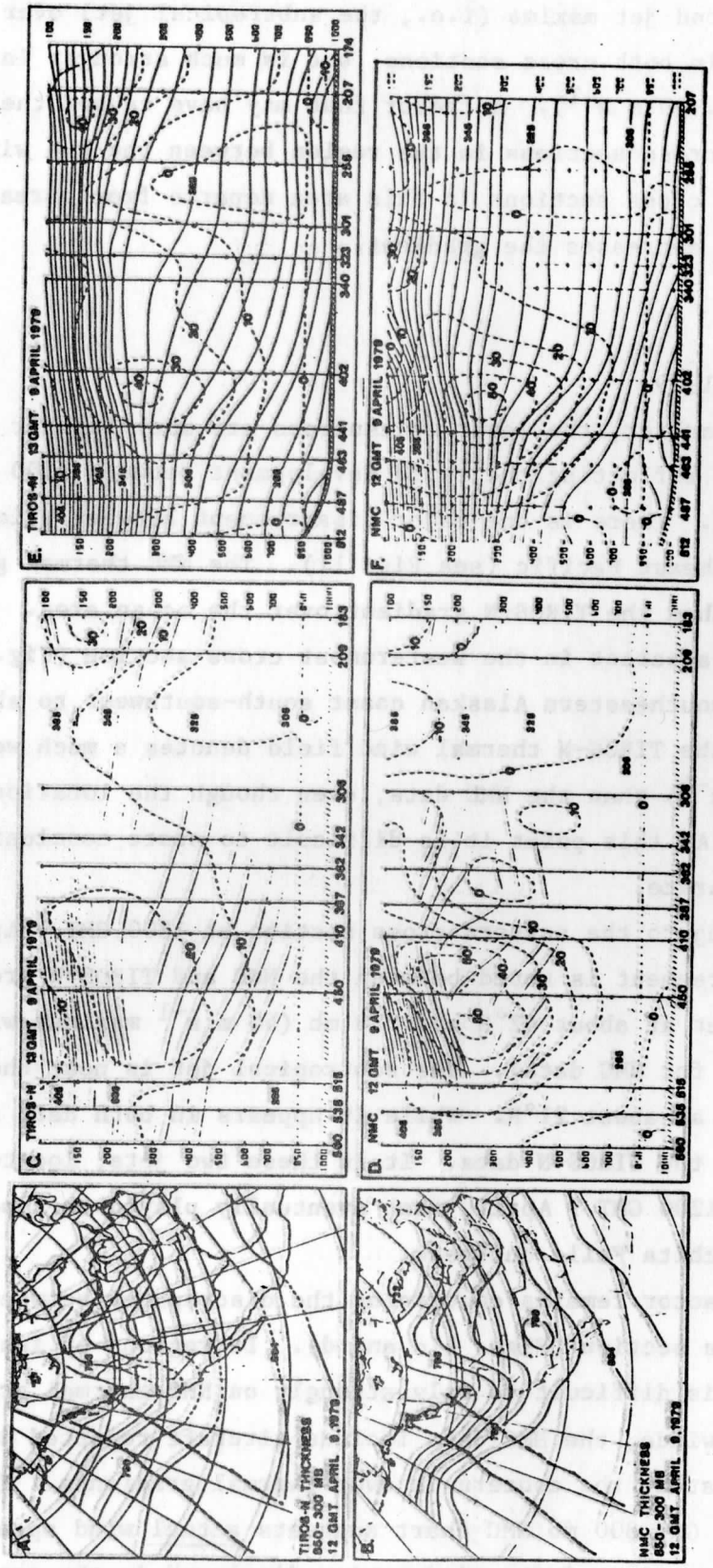

Fig. 11. Data format same as Fig. 8 except for 1200 GMT 9 April 1979.

about 50 m s^{-1} at 300 mb in the NMC data. Since the NMC analyses includes the effects of auxiliary data (e.g., aircraft winds) in computing the NMC thermal field, it may be superior to the TIROS-N data in this area.

To further compare the relative performance of TIROS-N and NMC data over oceanic areas devoid of radiosonde data, a small study was done comparing their relative performances over ocean and land areas. In this sub-study, absolute values of the 850-300 mb thickness values were calculated at each TIROS-N sounding location and the corresponding NMC location for all five data periods. The data were separated into two categories: land locations (i.e., where NMC analyses have abundant radiosonde data) and oceanic areas (i.e., where NMC has very limited radiosonde data). In all five time periods investigated, the differences between the TIROS-N and NMC thickness values were greater over the ocean than the land. The combined five periods showed differences of 28.7 meters over land and 38.9 meters over the ocean. In doing this comparison, no attempt was made to screen the TIROS-N data for obviously bad soundings. This tends to indicate that the NMC thickness data is likely to have greater errors over the ocean than TIROS-N, if one can assume that the TIROS-N errors are independent of location. In general, satellite soundings are relatively better over oceanic areas than in land regions, especially those with high terrain.

4) 1200 GMT 8 April 1979

A high degree of correlation between the NMC and TIROS-N thickness fields (Fig. 12a and b) is evident in the earliest period of this study, 1200 GMT 8 April. Lower thicknesses are located over the northern Plains and southern California where a short wave trough and closed low are positioned, respectively. Once again, the thermal gradient is weaker in the TIROS-N analysis over the northeast Pacific. The polar jet streak is well out over the Pacific in Fig. 12c and d, with the maximum winds at 42-43°N in both NMC and TIROS-N thermal wind fields. Slightly lower wind speeds (40 m s^{-1} vs. 50 m s^{-1}) are found in the polar jet for the TIROS-N cross section reflecting the weaker thickness gradient in this region. The subtropical jet maxima is shown in Fig. 12e and f over the Pacific near 19°N by a second cross section which extends southward to 12°N just off the maps of Fig. 12a and b. Both jet cores look more realistic in the TIROS-N wind fields, with centers near 200-300 mb rather than extending above 100 mb as in the NMC analyses.

In considering the five time periods described above, it is encouraging that the propagating wind maxima which were instrumental in the Wichita Falls outbreak could be traced back in time 60 hours to when the maximum winds, especially the

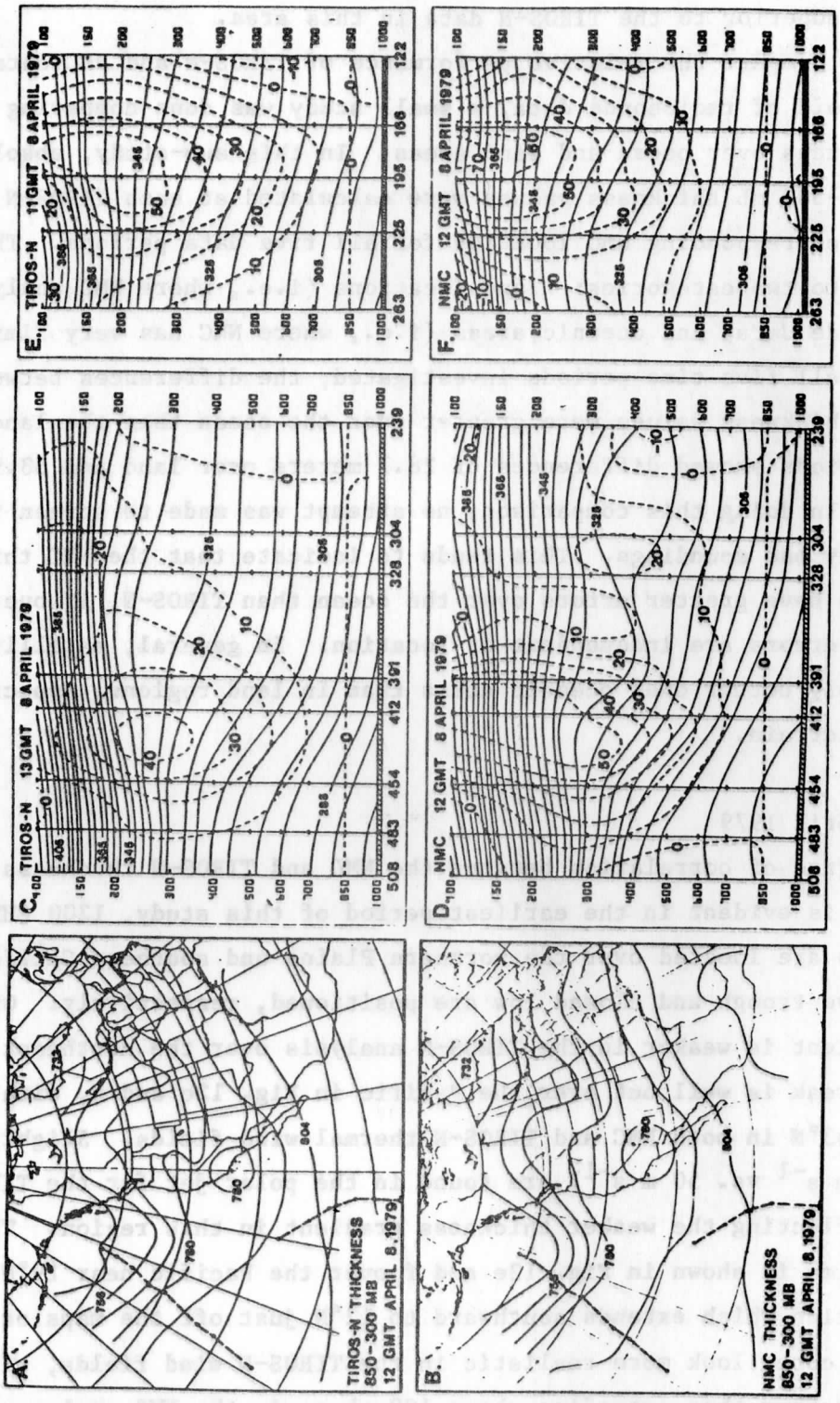

Fig. 12. Data format same as Fig. 8 except for 1200 GMT 8 April 1979.

polar jet, were located well out over the Pacific. At that earliest time, the polar jet maximum was located near 42 or 43°N, while the subtropical jet was located far to the south near 19°N. The subtropical jet is relatively more fixed in position than the polar jet. Even in the earliest period, the subtropical jet extended northeastward into the Mexican-Texas border area. As the polar jet propagated eastward and southward around the wave, the confluence of these wind maxima over west Texas very likely aided in the cyclone development. Downstream, their diffluence in eastern Texas (and the propagation of the polar jet into this area) contributed to the major weather disaster.

5. Conclusion

This study, which focused on the synoptic events preceding the Wichita Falls tornado outbreak of 10-11 April 1979, traced the principal wind maxima (subtropical and polar jets) involved in the outbreak back upstream for the prior three days. At that time they were located well out over the Pacific. The purpose was twofold: 1) to achieve a better description of how these wind maxima, widely separated over the Pacific, became confluent over western Texas and then diffluent over eastern Texas in the region of the severe weather, and 2) to investigate the ability of TIROS-N satellite soundings to reasonably locate the wind maxima over the relatively data void Pacific Ocean and Mexico.

Most previous studies that tested the reliability of satellite soundings have involved direct satellite - radiosonde comparisons usually employing isentropic cross sections. In this study, only a minimum of such comparisons were done. Rather, comparisons were made primarily between cross sections based on NMC analyses and TIROS-N soundings. In order to best position the various cross sections and to gain more general information on the thermal structure of the atmosphere, 850-300 mb thickness fields based on NMC analyses and TIROS-N data were also constructed and examined for each time period.

With respect to the first goal, the study did show the confluence of the subtropical and polar jets. From a location well out in the Pacific (140°W) on 8 April, when the two jets were over 20° latitude apart, they approached one another until 10 April when their jet cores were only separated by about 8° of latitude over west Texas. Only 500 km to the east, the two jets were 11° of latitude apart. Perhaps one of the most significant features was that the confluence was caused mainly by the polar jet streak plunging southward and around the developing wave over the western United States. The subtropical jet, oriented

approximately from west-southwest to east-northeast, showed a much smaller variation with time. This is in general agreement with the conventional view of a relatively steady subtropical jet.

Turning to the ability of the TIROS-N data to locate and track the wind maxima associated with the polar and subtropical jets, a somewhat more difficult problem was encountered. This problem arises primarily because of the lack of a reliable verification data set over the Pacific Ocean and Mexico. To partially circumvent this difficulty, radiosonde cross sections were constructed over the data rich United States. Comparison of these cross sections with similar ones based on TIROS-N and NMC analyses were done. Although not conclusive, these comparisons indicated that TIROS-N cross sections did as well as the NMC analysis cross sections in locating the thermal wind maxima associated with the polar and subtropical jets in this data rich area. In some respects, the TIROS-N thermal wind field showed better agreement with the radiosonde thermal wind field, especially in depicting a stronger, more vertically extensive polar jet and a single maximum in the subtropical jet.

In examining each time period prior to the tornado outbreak, both NMC and TIROS-N thickness fields and cross sections were used to define the thermal support of the jet streams. Thus, as noted earlier, it was possible to follow the wind maxima back in time. Although it certainly cannot be said unequivocally that TIROS-N cross sections provided a better description of the jets than the NMC cross sections, the TIROS-N data appeared to have notable advantages. TIROS-N cross sections consistently demonstrated the ability to resolve separate polar and subtropical jet maxima which could be tracked back in time over the Pacific, while the NMC cross sections often failed to depict these two distinct maxima. This was partially due to the smoothing of the data field employed in the NMC analyses. It should be noted that weaker winds in the TIROS-N cross sections, especially over the northeast Pacific, seem to be typical of the weaker gradients often found in satellite sounding fields. On the other hand, a possible advantage of TIROS-N data is that the same instrument was used in determining the satellite soundings, compared to the heterogeneous collection of observations used in data sparse regions of the NMC analysis (i.e., Pacific Ocean). Concentration of the thermal gradient near coastal areas where the transition in data availability occurred also appeared to bias the NMC analyses. NMC - TIROS-N comparisons of 850-300 mb thickness values over land areas and ocean areas showed consistently greater differences over the ocean areas. If the satellite sounding errors are assumed to be independent of location and since the NMC thickness values should be more accurate over the data

rich land areas, the NMC analyses may have had greater thickness errors over the ocean than TIROS-N data.

Overall, this study demonstrated that TIROS-N satellite data could be used to track jet maxima from well out over the Pacific and to depict the polar and subtropical jet streams at the time of the Wichita Falls tornado outbreak. However, drawing definite conclusions about the ability of satellite soundings in such endeavors based only on this single case may be somewhat over-optimistic.

Acknowledgements

The authors sincerely thank Dr. Thomas Koehler for his extensive support in solving various computing problems and for his general comments concerning certain facets of the research problems. Patricia Marvin, Kathi Marvin and Brian Jarvis were instrumental in preparing the various figures and Kathi Marvin and Eva Singer edited and typed the final manuscript. We are grateful for their assistance. This research was supported by NOAA Grant NA 79AA-H-00011.

References

Achtor, T.H., and L.H. Horn, 1981: Spring season Colorado cyclogenesis. Part I: Evidence of the coupling of the upper tropospheric jet streak to the low level jet. Synoptic-Dynamic Applications of Meteorological Satellite Data, Final Report, NOAA Grant NA 79AA-H-00011, Dept. of Meteorology, Univ. of Wisc.-Madison.

Bergman, K.H., 1979: Multivariate analysis of temperatures and winds using optimum interpolation. Mon. Wea. Rev., 107, 1423-1444.

Blechman, A.G., and L.H. Horn, 1981: The influence of higher resolution Nimbus-6 soundings in locating jet maxima. Case Studies Employing Satellite Indirect Soundings, Final Report, NOAA Grant 04-4-158-2, Dept. of Meteorology, Univ. of Wisc.-Madison.

Bleck, R., and P.L. Haagenson, 1968: Objective analysis on isentropic surfaces. NCAR Tech. Notes, NCAR-TN-39, Boulder, Colo., 27 pp.

Cahir, J.J., 1971: Implications of circulations in the vicinity of jet streaks at subsynoptic scales. Ph.D. Thesis, Penn. State Univ., 170 pp.

Duquet, R., E.F. Danielsen, and N.R. Phares, 1966: Objective cross section analysis. J. Appl. Meteor., 5, 233-245.

Horn, L.H., R.A. Petersen, and T.M. Whittaker, 1976: Intercomparisons of data derived from Nimbus-5 temperature profiles, rawinsonde observations and initialized LFM model fields. Mon. Wea. Rev., 104, 1362-1371.

Hovanec, R.D., and L.H. Horn, 1975: Static stability and the 300 mb isotach field in the Colorado cyclogenetic area. Mon. Wea. Rev., 103, 628-638.

Kapela, A., and L.H. Horn, 1975: Nimbus-5 satellite soundings in a strongly baroclinic region. Meteorological Applications of Satellite Indirect Soundings, Project Report, NOAA Grant 04-4-158-2, Dept. of Meteorology, Univ. of Wisc.-Madison.

Marshment, R.A., and L.H. Horn, 1981: Spring season Colorado cyclogenesis. Part II: Distribution of atmospheric water vapor and its influence on static stability. Synoptic-Dynamic Applications of Meteorological Satellite Data, Final Report, NOAA Grant NA 79AA-H-00011, Dept. of Meteorology, Univ. of Wisc.-Madison.

McPherson, R.D., K.H. Bergman; R.E. Kistler, G.E. Rasch, and D.S. Gordon, 1979: The NMC operational global data assimilation system. Mon. Wea. Rev., 107, 1445-1461.

Palmén, E., and C.W. Newton, 1969: Atmospheric Circulation Systems, Academic Press, New York, 603 pp.

Sechrist, F.S., and T.M. Whittaker, 1979: Evidence of jet streak vertical circulations. Mon. Wea. Re., 107, 1014-1021.

Smith, W.L., H.B. Howell, and H.M. Woolf, 1979: The use of interferometric radiance measurements for sounding the atmosphere. J. Atmos. Sci., 36, 566-575.

Smith, W.L., and H.M. Woolf, 1976: The use of eigenvectors of statistical covariance matrices for interpreting satellite sounding radiometer observations. J. Atmos. Sci., 33, 1127-1140.

Togstad, W.E., and L.H. Horn, 1974: An application of the satellite indirect sounding technique in describing the hyperbaroclinic zone of a jet streak. J. Appl. Meteor., 13, 264-276.

Uccellini, L.W., and D.R. Johnson, 1979: The coupling of upper and lower tropospheric jet streaks and implications for the development of severe convective storms. Mon. Wea. Rev., 107, 682-703.

Whitney, L.F., 1977: Relationship of the subtropical jet stream to severe local storms. Mon. Wea. Rev., 105, 398-412.

Whittaker, T.M., and R.A. Petersen, 1977: Objective cross-sectional analyses incorporating thermal enhancement of the observed winds. Mon. Wea. Rev., 105, 147-153.

Spring Season Colorado Cyclogenesis. Part I: Evidence of the Coupling of the Upper Tropospheric Jet Streak to the Low Level Jet

Thomas H. Achtor* and Lyle H. Horn

Department of Meteorology, University of Wisconsin
Madison, Wisconsin 53706

Abstract

A set of 71 cases of spring season (April and May) Colorado cyclogenesis obtained from Hovanec and Horn (1975) is used to examine the relationship between the upper tropospheric westerly jet streak and the southerly low level jet (LLJ). Of the 71 cases 32 failed to develop while 39 fully developed. A composite approach was used to reveal the primary characteristics of the two samples. A total of six rawinsonde observation periods more-or-less centered around the time of cyclogenesis were used in the study.

The developing sample (D) composite shows a nearly classical 300 mb jet streak propagating into the Southern Plains; while the non-developing (ND) composite shows a disorganized wind pattern at 300 mb. A composite based on a subset consisting of 15 days on which a well defined jet streak (JS) was present in west Texas was selected from the 32 developing cases. As expected, the JS composite showed enhanced jet streak characteristics.

In the developing (D) and jet streak (JS) composites pronounced 850 mb wind maxima are located beneath the exit region of the 300 mb jet streak, with the axes of the two jets crossing at a large angle, especially at 0000 GMT. Ageostrophic winds were calculated for both the 300 and 850 mb levels. Those at 300 mb were divided into tangential and normal components. The results support the existence of an indirect circulation in the exit region of the 300 mb jet and indicate that the low level southerly branch of the indirect circulation is important to the development of the LLJ.

---

*Present affiliation
Space Science and Engineering Center
University of Wisconsin, Madison, WI 53706

1. Introduction

This paper (Part I) presents evidence relating the upper tropospheric jet and low level jet commonly observed in cases of developing Colorado cyclones. In the following paper (Part II), Marshment and Horn (1981) use the same cases to examine the moisture distribution during cyclone development, particularly noting its significant role in reducing static stability and thus contributing to severe weather events.

Meteorologists have long realized that the region in which the westerly polar jet stream crosses the southerly low level jet (LLJ) is a preferred area for outbreaks of severe local weather. Nearly thirty years ago, Fawbush and Miller (1953, 1954) noted that the veering of the wind with height in this region results in the advection of cooler, drier air from the west at higher elevations, a condition favoring deep convection. This synoptic pattern, illustrated in Figure 1 from Newton (1967), is commonly associated with developing Colorado cyclones.

For many years both the polar jet and LLJ have been studied as mechanisms which favor the development of deep convection, but most studies concentrated on either one or the other and not their combination. See, for example, Reiter (1963) and Newton (1967) for discussions involving the upper tropospheric jet, and Means (1952, 1954) and Bonner (1968) for discussions of the role of LLJ. Beebe and Bates (1955) did note that the crossing of the two jets could lead to patterns of convergence and divergence which induce vertical motion. Earlier, Murray and Daniels (1953) described the existence of a transverse indirect circulation in the exit region of an upper tropospheric wind maximum (also referred to as a jet streak) and a direct circulation in the entrance region. The transverse circulations include vertical motions which can produce or inhibit convection. The lower branch of the indirect circulation in the exit region can be viewed as contributing to the southerly flow and LLJ.

Cahir (1971) employing a vertical plane two-dimensional primitive equation model, clearly simulated the existence of a transverse indirect circulation in the exit region of a jet streak. (See Fig. 2 in Uccellini and Johnson, 1979.) Uccellini and Johnson (1979), using a hybrid isentropic sigma coordinate model simulated a propagating jet streak and accompanying mass adjustments which are in agreement with a transverse indirect circulation in the exit region of the jet. The mass adjustments are also consistent with the development of an isallobaric wind component on lower isentropic surfaces which enhances a southerly LLJ. In addition

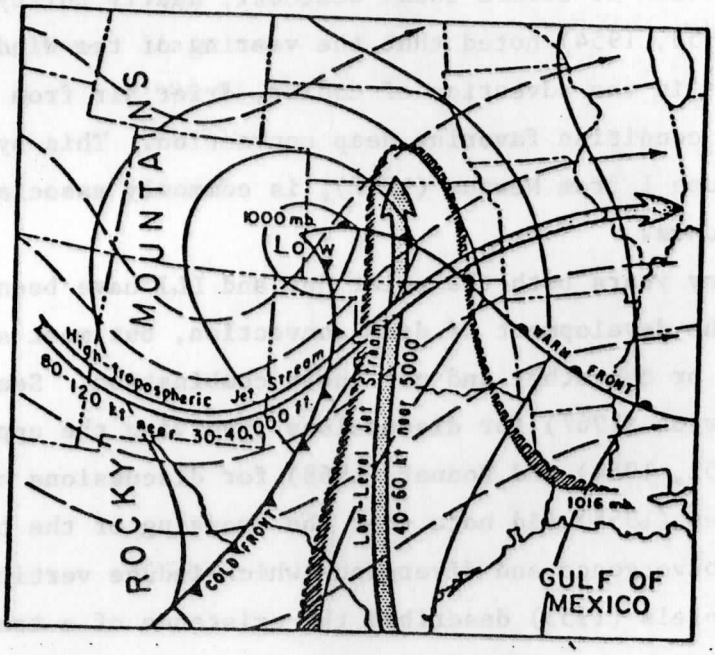

Fig. 1. Schematic Colorado cyclone, upper and lower tropospheric jets and moist tongue. (From Newton, 1967)

to their modelling results, they note individual synoptic cases which support their contention of a coupling of the upper tropospheric and low level jets. Uccellini (1980) has provided additional evidence of the coupling in individual situations.

Because a distinct nocturnal maximum exists in the LLJ, much of the previous work has focused on the diurnal variation of the LLJ itself and not on the larger synoptic pattern aloft. Blackadar (1957) proposed that the decrease of convective turbulence at night decouples the wind above the boundary layer from the wind at lower levels producing a maximum just above the stable layer. He further suggests that the nocturnal increase in the wind speed leads to an inertial oscillation in the wind field. Lettau (1967) has noted that nocturnal radiational cooling from the surface of the sloping terrain of the Great Plains produces a horizontal temperature gradient. By the thermal wind concept, this leads to an increased nighttime southerly wind component several hundred meters above the surface.

In this study, the relationship between the upper tropospheric jet streak and the LLJ is examined using a composite approach. The approach and data follow directly from Hovanec and Horn (1975), who used a data sample consisting of days on which Colorado cyclogenesis occurred. In preparing a composite (or mean) map of the 300 mb flow based on 39 days of significant spring season Colorado cyclogenesis, they found a distinct, almost classical, 300 mb jet streak in the Colorado region. Nearly all the cases of surface cyclogenesis occurred in the left front quadrant of the jet streak, the ascending branch of the indirect cell. For this study the same days (i.e.,events) of spring season Colorado cyclogenesis are employed; however, the data sample has been expanded from two to six rawinsonde time periods. In addition, 300 and 850 mb height data and 850 mb observed winds are also employed. (Hovanec and Horn used only 300 mb observed wind speed data.) The inclusion of the 850 mb data makes it possible to examine the LLJ on days of Colorado cyclogenesis. Moreover, the inclusion of geopotential height data makes it feasible to calculate the ageostrophic wind components which help define the transverse circulation. By employing a composite approach it is possible to gain insight into some of the basic characteristics of the jet streaks associated with Colorado situations. Studies of individual cases sometimes suffer because no two cases are identical. Focusing on a composite is more likely to reveal features which are common to the cases within the sample. Another advantage of this approach is that measurement errors that might contaminate individual studies are damped in composite studies. In a sense, the composite approach can be viewed as a type of climatology based on the means of events rather than on means obtained over some continuous period of time.

2. Selection of cyclogenetic events

The data sample used here is based on spring (April-May) events of Colorado cyclogenesis for the years 1964-1971. Hovanec and Horn (1975) used the Daily Weather Map series to determine cyclogenesis, which was defined as the location and time of occurrence of a closed sea level pressure isobar (4 mb interval) on the surface chart, provided it persisted for at least 24 hours. A total of 71 spring cases were found. These were classified as either developing (D), if they maintained a closed isobar for 72 hours, or non-developing (ND), if they did not. Figure 2 shows the partitioning of the spring season sample. Note that there were 39 developing (D) and 32 non-developing (ND) cases. The surface maps used to determine cyclogenesis (i.e., the first closed isobar) were for 0600GMT for 1964-68 and 1200GMT for 1968-1971. As previously noted, the data sample used here was expanded to include six radiosonde observation times with the total period of the study more-or-less centered around the time of cyclogenesis. The various calculations done are for 0000 and 1200 GMT on the day of cyclogenesis, called day C and for the preceding and following days, called days C-1 and C+1, respectively.

Because Hovanec and Horn selected their sample on the basis of Colorado cyclogenesis and not on whether a jet streak was present, a subsample of 15 days was subjectively chosen from the 39 developing days when a jet streak was located over or near the western Texas area on day C. This subset, referred to as the JS sample, was expected to enhance the features found in the developing sample. It should be kept in mind, however, that the JS and D sets are not independent.

3. Procedures

To better understand the significance of jet streaks and their relation to the LLJ in cases of Colorado cyclones, the mean observed and ageostrophic wind fields at 300 and 850 mb were obtained for each sample (ND, D, JS). The mean observed wind fields for each 0000 and 1200 GMT period were obtained by calculating the mean eastward and northward wind components at each rawinsonde station, and interpolating these components to a 2 x 2° latitude-longitude grid using the Barnes (1964) method.

Mean ageostrophic wind fields were obtained from the mean observed and geostrophic wind differences at the grid points. The geostrophic winds were calculated from mean geopotential height fields interpolated to the 2° x 2° latitude-longitude grid from the mean heights at each station. These heights at the station were computed hydrostatically using 50 mb increment temperatures and not

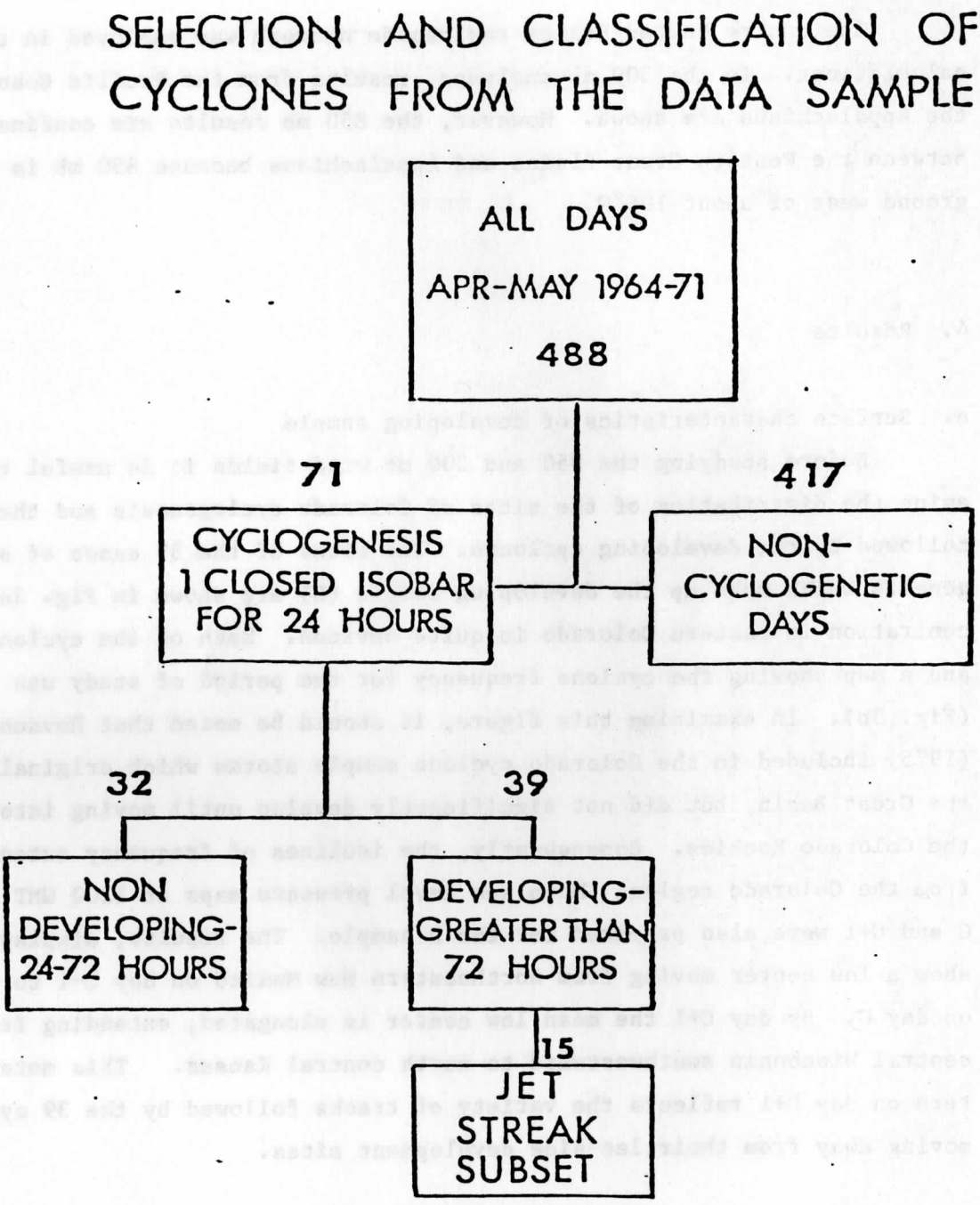

Fig. 2. Partitioning of the April-May 1964-71 cyclogenesis cases. Numbers show the total days in each group.

from the reported heights. As will be described later, the ageostrophic wind at each grid point was partitioned into components normal and tangential to the mean wind at the grid point.

The entire United States rawinsonde network was employed in the above calculations. In the 300 mb analyses, results from the Pacific Coast eastward to the Appalachians are shown. However, the 850 mb results are confined to the area between the Western Great Plains and Appalachians because 850 mb is often below ground west of about 105°W.

4. Results

a. Surface characteristics of developing sample

Before studying the 850 and 300 mb wind fields it is useful to briefly examine the distribution of the sites of Colorado cyclogenesis and the tracks followed by the developing cyclones. The sites of the 39 cases of surface cyclogenesis which make up the developing sample (D) are shown in Fig. 3a. The concentration in eastern Colorado is quite obvious. Each of the cyclones was tracked and a map showing the cyclone frequency for the period of study was prepared (Fig. 3b). In examining this figure, it should be noted that Hovanec and Horn (1975) included in the Colorado cyclone sample storms which originally formed in the Great Basin, but did not significantly develop until moving into the lee of the Colorado Rockies. Consequently, the isolines of frequency extend westward from the Colorado region. Mean sea level pressure maps at 1200 GMT for days C-1, C and C+1 were also prepared for the D sample. The results, displayed in Fig. 4, show a low center moving from northeastern New Mexico on day C-1 to western Kansas on day C. By day C+1 the mean low center is elongated, extending from west central Wisconsin southwestward to north central Kansas. This more diffuse pattern on day C+1 reflects the variety of tracks followed by the 39 cyclones after moving away from their lee-side development sites.

b. Observed wind fields at 300 and 850 mb.

Mean observed wind fields for 300 and 850 mb were prepared (ND, D, JS) for three consecutive time periods (1200 GMT of day C-1, and 0000 GMT and 1200 GMT of day C), but for the ND sample only the two 1200 GMT periods were done. The results are presented in Figures 5-7. The streamlines in these figures were objectively constructed from the mean wind component analyses using an automated technique

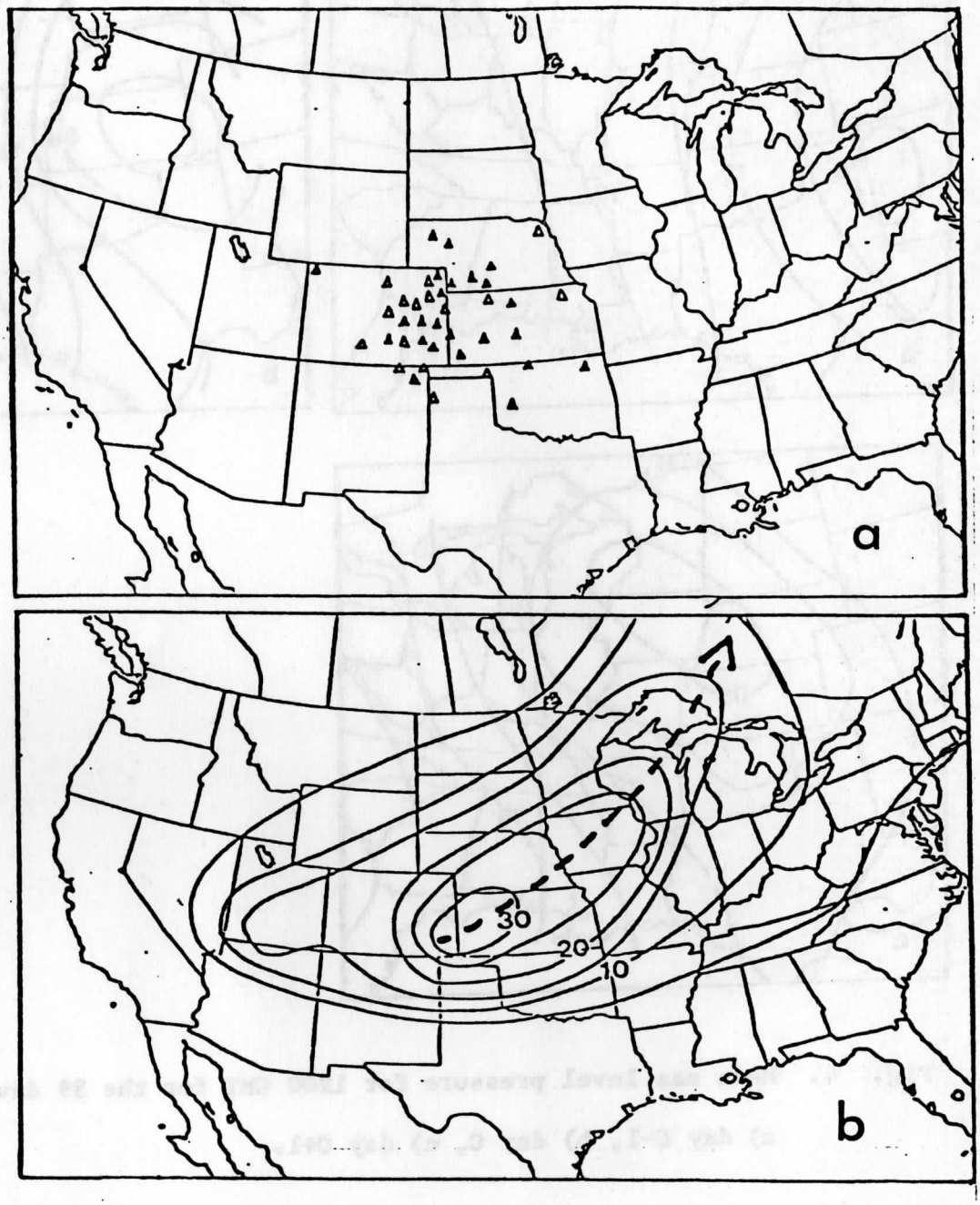

Fig. 3. a) Sites of the 39 cases of developing cyclones. Solid triangles are for those used in the JS sample.

b) Cyclone frequency based on the 39 cases. Heavy dashed line indicates mean cyclone track.

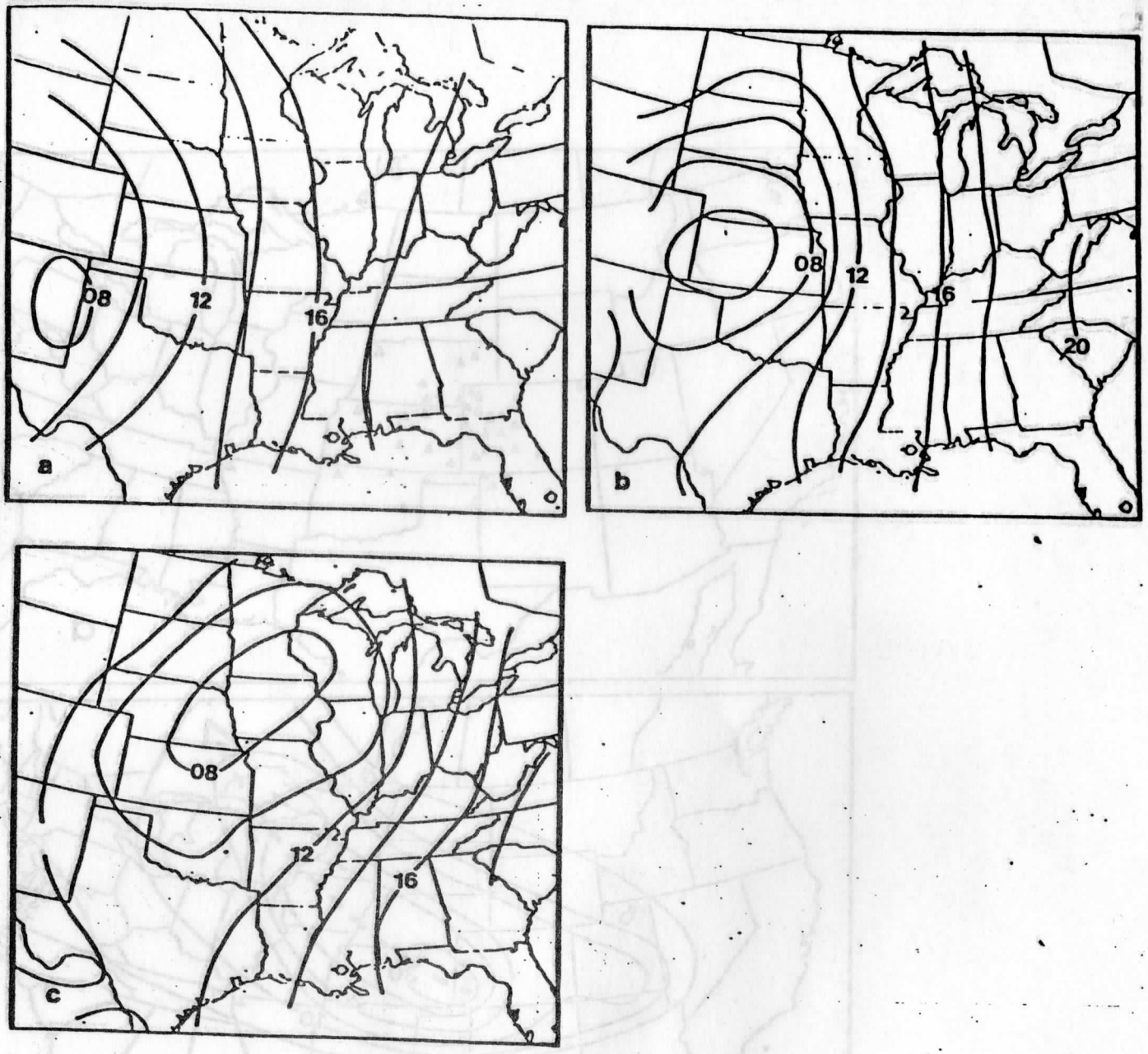

Fig. 4. Mean sea level pressure for 1200 GMT for the 39 developing cases. a) day C-1, b) day C, c) day C+1.

Fig. 5. Mean isotachs and streamlines for the three samples for 1200 GMT, day C-1 a) 300 mb, ND; b) 850 mb ND; c) 300 mb D; d) 850 mb D; e) 300 mb JS; f) 850 mb JS.

Fig. 6. Mean isotachs and streamlines fore 0000 GMT, day C. a) 850 mb ND; b) 300 mb D; c) 850 mb D, d) 300 mb JS; e) 850 mb JS.

Fig. 7. Same as Fig. 5 except for 1200 GMT, day C

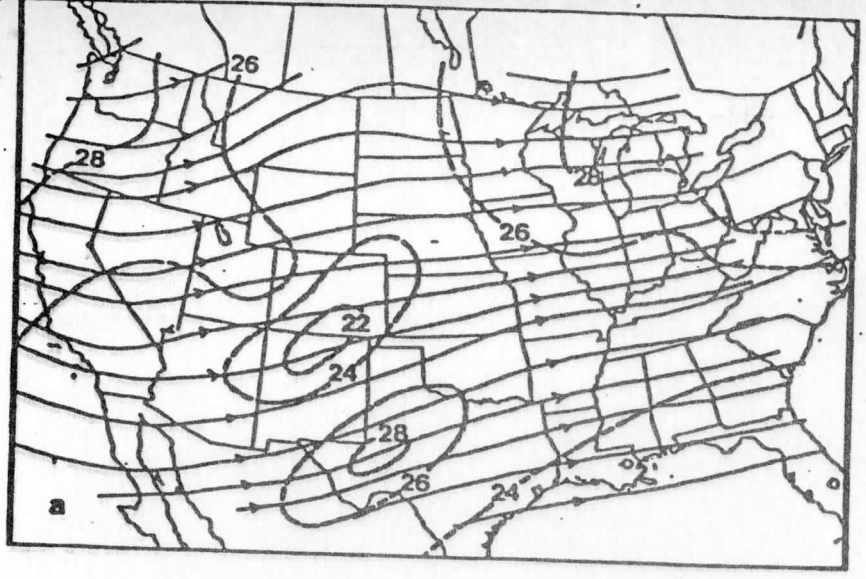
26
28
26
22
24
28
26
24
a

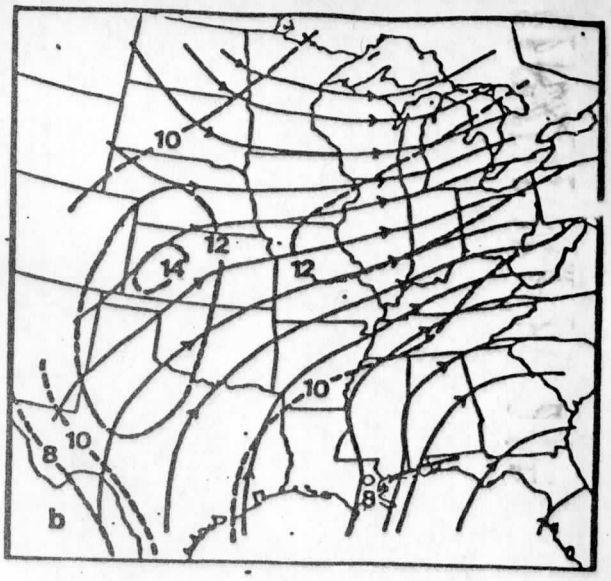
10
12
14
12
10
10
8
8
b

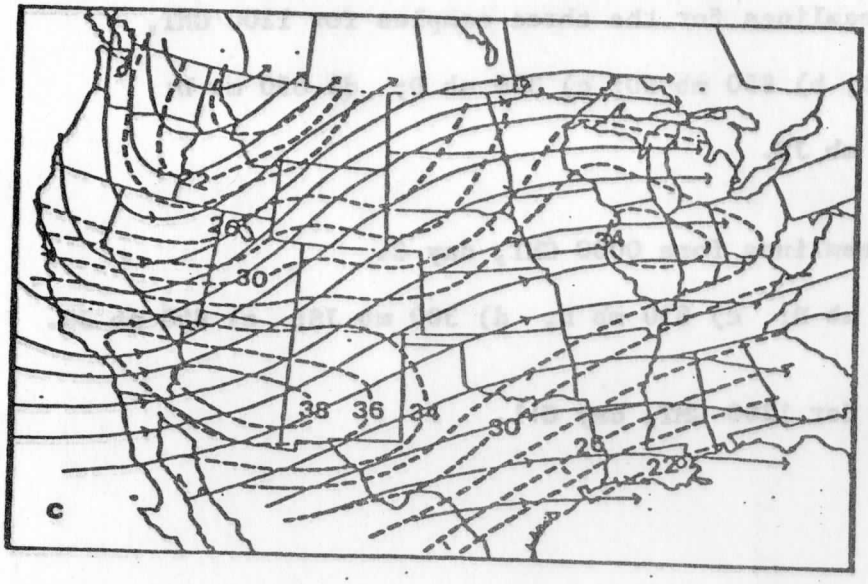
22
36
34
30
38
36
34
30
26
22
c

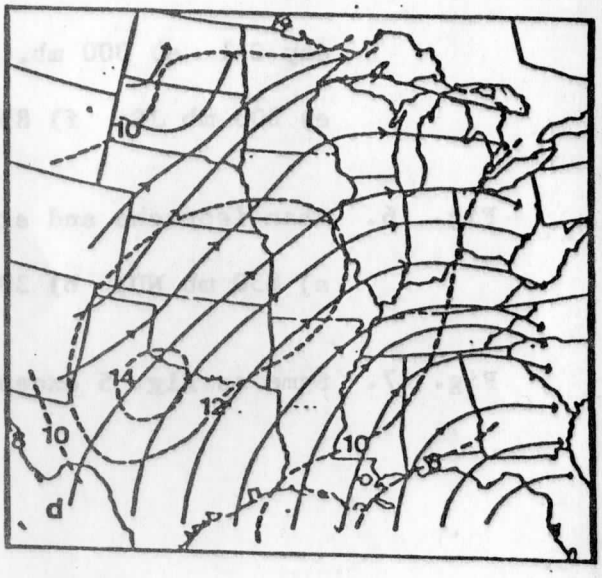
10
14
12
10
8
10
d

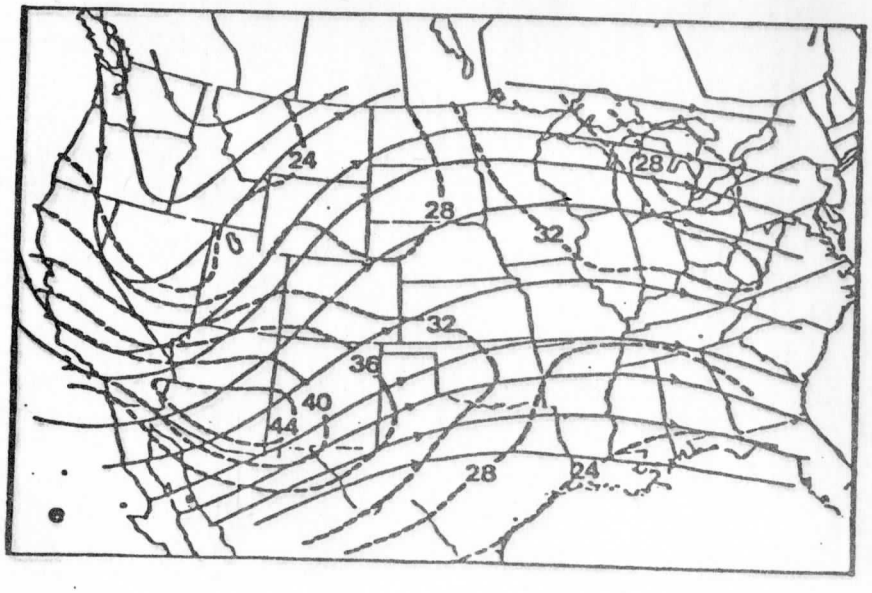
24
28
28
32
32
36
40
44
28
24
e

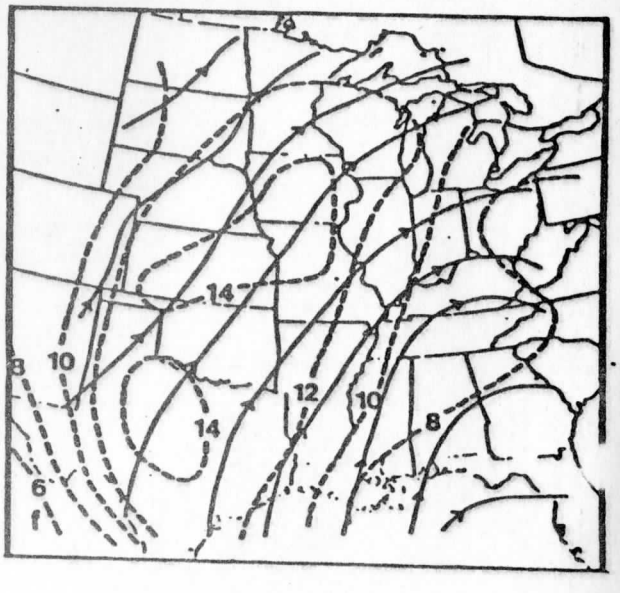
14
10
8
14
12
10
8
6
f

Fig. 5

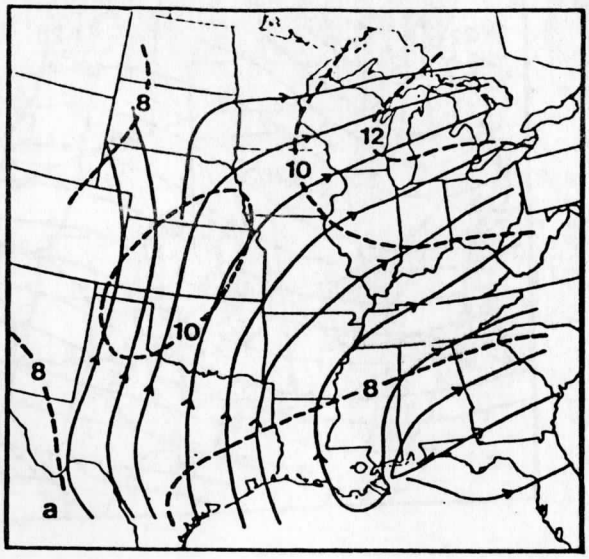
8
12
10
10
8
8
a

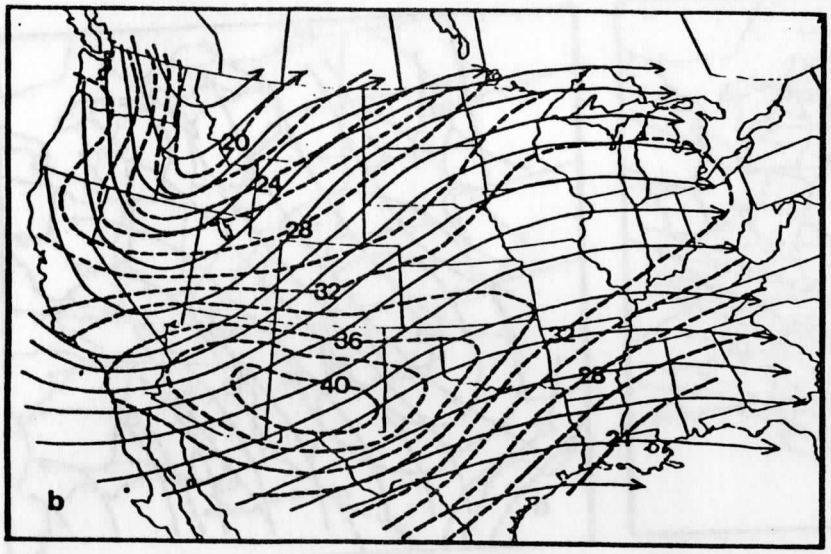
20
24
28
32
36
40
28
24
b

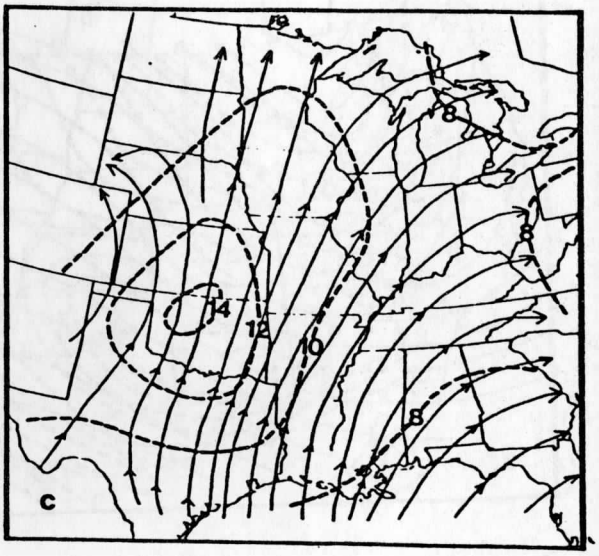
8
14
12
10
8
c

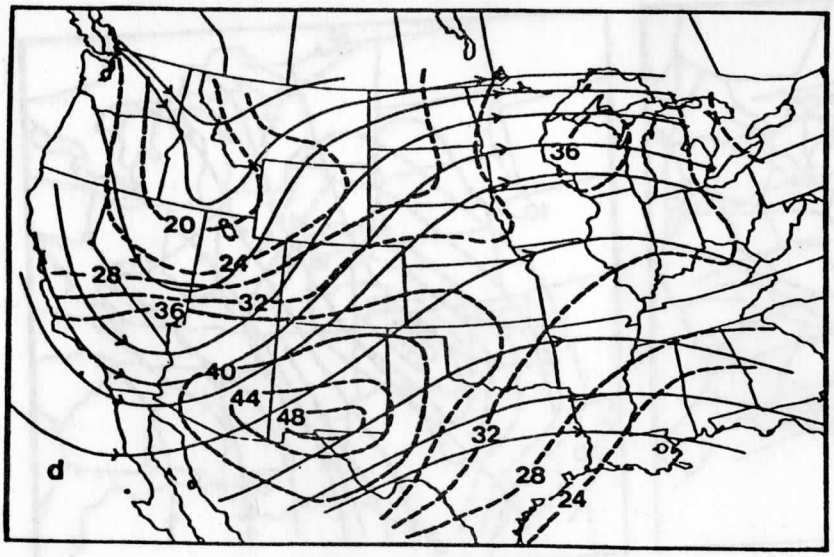
36
20
28
24
36
32
40
44
48
32
28
24
d

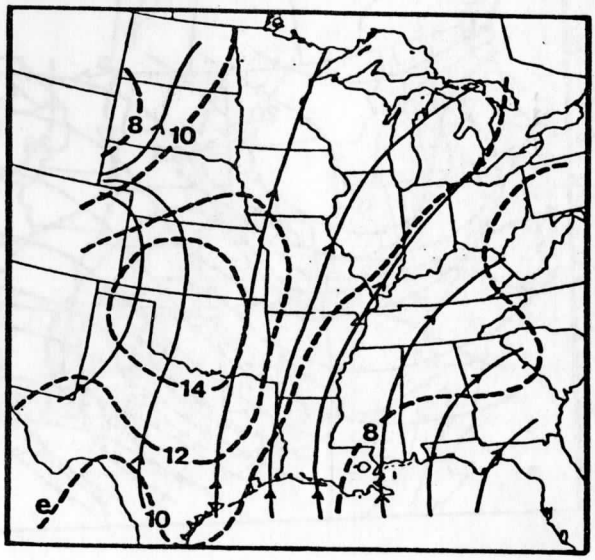
8
10
14
12
10
8
e

Fig. 6

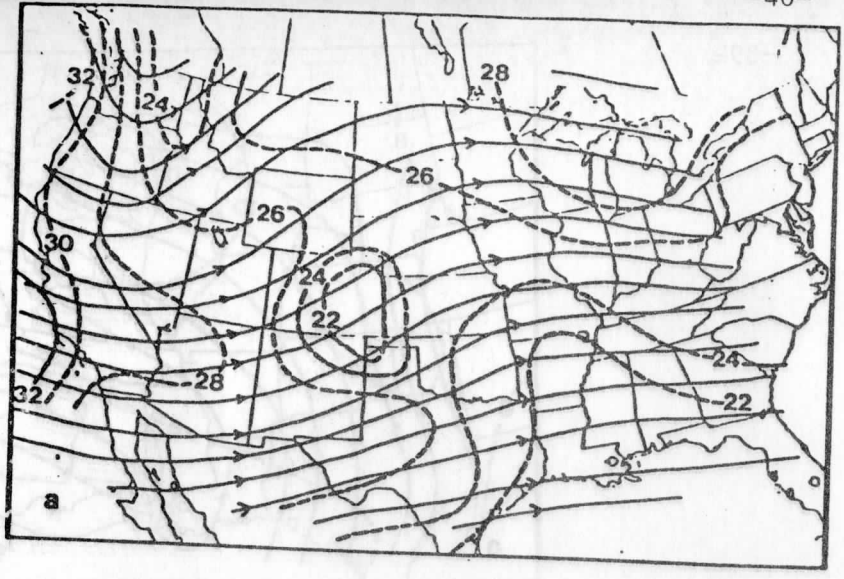
32
24
28
26
26
30
24
22
28
24
32
22
a

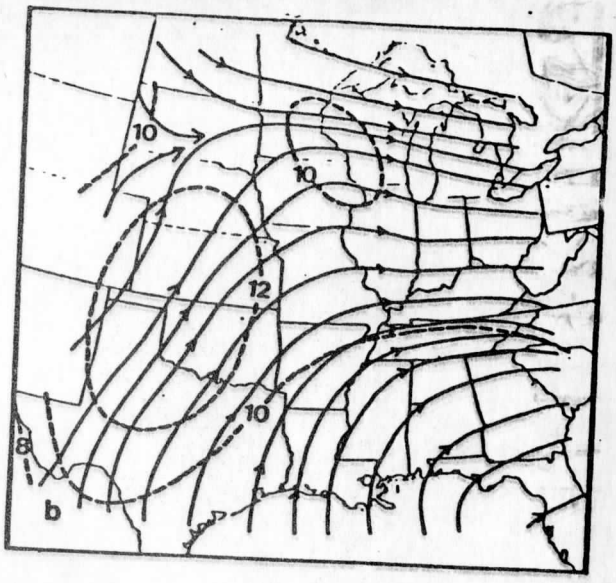
10
10
12
10
8
b

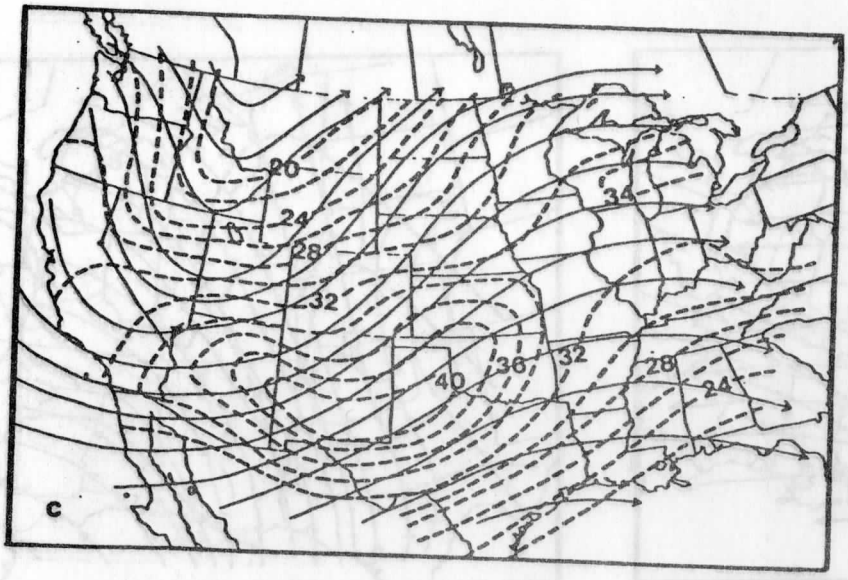
20
24
28
32
34
40
36
32
28
24
c

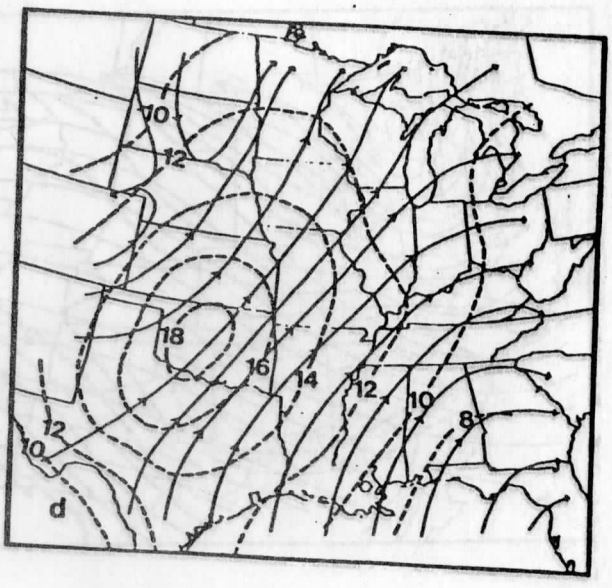
10
12
18
16
14
12
10
8
12
10
d

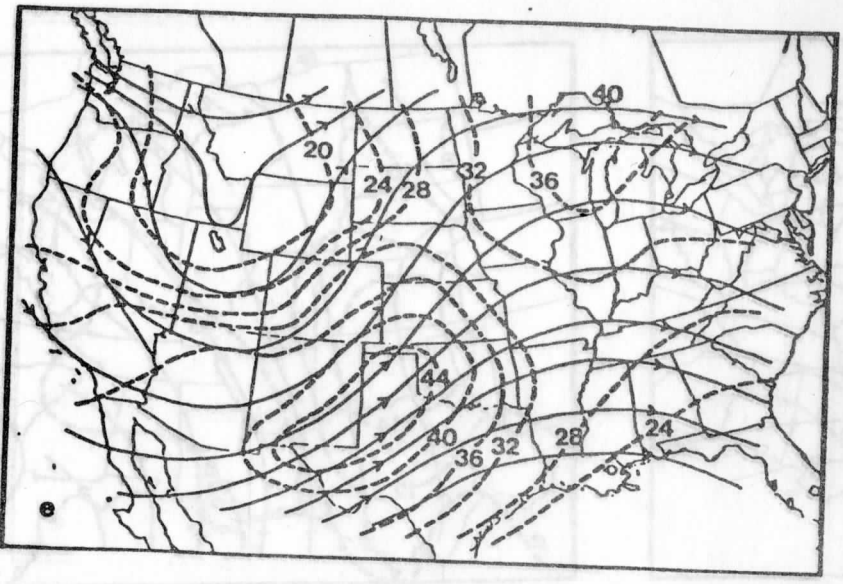
40
20
24
28
32
36
44
40
36
32
28
24
e

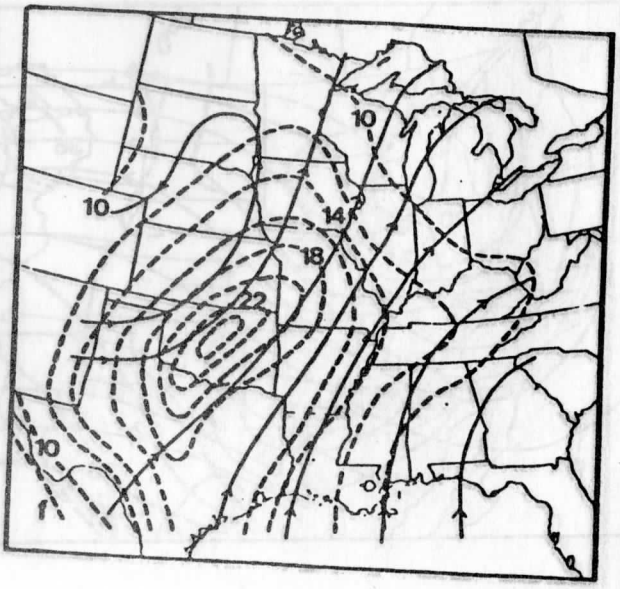
10
10
14
18
22
10
f

Fig. 7

devised by Whittaker (1977). However, the isotach fields shown were hand analyzed using the mean of the reported wind speeds at each station. Although wind analyses were prepared for all six time periods, the results for these three time periods show the most significant features. Note the distinct differences between the 300 mb fields for the non-developing (ND) sample and the other two samples (D and JS). For the time periods shown, the ND 300 mb wind fields (Figs. 5a, 7a) fail to show any significant isotach maximum near the eastern Colorado cyclogenesis area. (The 300 mb wind field for 0000 GMT, day C was not constructed.) In contrast, the D and JS means show distinct, almost classical, 300 mb jet streaks in the southwestern United States which propagate eastward during the three time periods. The JS wind maxima are somewhat stronger and more compact than the D maxima. This is to be expected since the 15 cases of the JS sample were selected from the D sample on the basis of a well developed jet streak in the area of western Texas. Recall the D sample was selected by Hovanec and Horn (1975) on the basis of cyclogenesis without regard to 300 mb wind data.

The 300 mb streamline patterns shown in Figs. 5-7 all indicate a mean eastward propagating trough in the western United States. However, the trough in the ND cases (Figs. 5a, 7a) has a smaller amplitude than in the D and JS samples, as expected, with the lack of significant development in the ND sample. Furthermore, a comparison of the 300 mb wind maxima (D sample) with the sites of cyclogenesis shown in Fig. 3a reveals that the large majority of the cyclones formed in the left front quadrant of the mean jet streak, within the area of the rising branch of the transverse indirect circulation. This is consistent with the concept of mass transport from the left to the right side of the jet by the upper branch of the circulation.

The 850 mb wind fields displayed in the right hand columns of Figs. 5-7 show only small differences between the ND sample and the D and JS samples for the first time period (1200 GMT, Day C-1). While the ND sample shows indications of a weak trough over the western Great Lakes, the D and JS sample show southwesterly flow over most of the central United States. All three samples show isotach maxima of 14 m s^{-1} over some portion of the Great Plains. These maxima probably reflect stronger winds due to nocturnal influences as described by Blackadar (1957) and Lettau (1967). Also note that at this time (1200 GMT, day C-1), the exit region of the 300 mb jet maxima (D, JS samples) was still located over western New Mexico, far to the west of the Colorado cyclogenetic area.

By 0000 GMT of day C, the 300 mb wind maxima (D and JS samples) had propagated eastward, with the exit region of jet streak now located over eastern New

Mexico and extreme western Texas. The 850 mb wind maxima, although only 14 m s^{-1}, is better organized than in the previous period. Since at 0000 GMT (late afternoon local time) vigorous turbulent mixing is present in the boundary layer, the surface frictional influence is probably present at 850 mb, especially over higher terrain. If this influence were not present, the 850 wind maxima would probably have exceeded 14 m s^{-1}. Also note that the 850 mb streamlines have a more north-south orientation at 0000 GMT than at the 1200 GMT bracketing times. Compare, for example, Fig. 6c with 5d and 7d. This turning of the wind from a more southerly component at 0000 GMT to a more southwesterly component at 1200 GMT likely represents the effect of an inertial oscillation introduced by the increased nighttime wind speeds.

By 1200 GMT of day C, the mean 300 mb jet streak continued to propagate eastward, with the exit region located over the southern plains (Figs. 7c and 7e). Below the exit region, 850 mb wind maxima of 18 and 24 m s^{-1} are present for the D and JS samples, respectively (Figs. 7d and 7f). In contrast, the ND case, which lacks a 300 mb jet streak, also lacks an 850 mb wind maxima (Fig. 7b). The considerably stronger 850 mb values for the JS sample reflects the selection of 15 cases from the D sample in which 300 mb jet streaks were present in the western Texas area. (Note that in selecting these 15 cases, no attention was given to the 850 mb wind data.) To offer a better visualization of the relationship between the 300 and 850 mb winds of the D sample, Fig. 8 was prepared. The 850 mb wind maxima is clearly, almost ideally, located beneath the exit region of the 300 mb jet streak. The 300 and 850 mb streamlines intersect at about a 45° angle. Had the observation been for 0000, rather than 1200 GMT, the angle would likely have been considerably larger, but the wind speeds at 850 mb would have been weaker. A similar diagram prepared for the JS sample using data from Figs. 7e and 7f, would present a similar pattern, but with stronger wind speed values. The relationships presented in Figs. 5-8 provide support for the Uccellini and Johnson (1979) and Uccellini (1980) contention that the LLJ represents the lower branch of the exit region indirect circulation.

c. Ageostrophic wind fields

Additional insight into the relationship between the 300 and 850 mb wind maxima and the role of the transverse indirect circulation in their coupling can be obtained by studying the ageostrophic wind components present in the D and JS samples. Maps displaying the ageostrophic wind fields at 300 and 850 mb are shown in Figs. 9-10. To aid in interpreting these fields, it is convenient to partition the 300 mb ageostrophic wind (V_{ag}) into its normal and tangential components and

Fig. 8. A few 850 mb isotachs and streamlines superimposed on some 300 mb isotachs and streamlines for the D sample at 1200 GMT, day C.

to examine the various processes which contribute to each.

Using the horizontal vector equation of motion in natural coordinates and the definition of the ageostrophic wind as the difference between the horizontal ($\underset{\sim}{V}_H$) and geostrophic wind ($\underset{\sim}{V}_g$) vectors it can be shown that,

$$\underset{\sim}{V}_{ag} = \frac{1}{f}\,\underset{\sim}{k} \times \left[\frac{\partial \underset{\sim}{V}_g}{\partial t} + \frac{\partial \underset{\sim}{V}_{ag}}{\partial t} + V_H \frac{\partial V_H}{\partial s}\,\underset{\sim}{t} + \frac{V_H^2}{R}\,\underset{\sim}{n} + w \frac{\partial \underset{\sim}{V}_H}{\partial z} - \alpha \frac{\partial \underset{\sim}{\tau}}{\partial z}\right] \tag{1}$$

where $\underset{\sim}{k}$, $\underset{\sim}{t}$ and $\underset{\sim}{n}$ are the unit vectors in the vertical, tangential and normal directions, f the coriolis parameter, s distance in the $\underset{\sim}{t}$ direction, R streamline curvature, z vertical distance, w vertical component of the wind velocity, α specific volume, and $\underset{\sim}{\tau}$ the frictional stress. Above the boundary layer, the largest contributors to $\underset{\sim}{V}_{ag}$ are the isallohypsic ($\frac{\partial \underset{\sim}{V}_g}{\partial t}$), the speed advection ($V_H \frac{\partial V_H}{\partial s}\,\underset{\sim}{t}$) and the curvature ($\frac{V_H^2}{R}\,\underset{\sim}{n}$) terms. Thus, the tangential component of $\underset{\sim}{V}_{ag}$ is produced primarily by the isallohypsic and curvature terms, while the normal component results from the speed advection and isallohypsic terms.

The combination of the speed advection and curvature terms is equivalent to the diadic product (i.e., the advective acceleration) in the horizontal vector equation of motion

$$V_H \frac{\partial V_H}{\partial s}\,\underset{\sim}{t} + \frac{V_H^2}{R}\,\underset{\sim}{n} = (\underset{\sim}{V}_H \cdot \nabla)\underset{\sim}{V}_H \tag{2}$$

The diadic product can be calculated directly from the mean u and v components and can be partitioned into normal and tangential components by forming the appropriate scalar products. The third major contributor to $\underset{\sim}{V}_{ag}$ (the isallohypsic term, $\frac{\partial \underset{\sim}{V}_g}{\partial t}$) was estimated using 24 hour height changes (12 hours before and after the time period studied).

Calculations at 300 mb for the D sample showed that the diadic product was between five and ten times larger than the isallohypsic term. Thus, it was assumed that at 300 mb the primary contribution to the tangential component of the ageostrophic wind is given by the curvature term and to the normal component by the alongstream speed advection term.

Similar calculations at 850 mb indicated that the diadic product was only about twice the size of the isallohypsic term, indicating that at 850 mb the isallohypsic term is relatively more significant than at 300 mb. Thus, it is not feasible to clearly relate the components of the 850 mb ageostrophic wind to the curvature and speed advection terms. Moreover at 850 mb, especially at 0000 GMT, the frictional term is undoubtedly an important contributor to $\underset{\sim}{V}_{ag}$.

In Fig. 9 the 300 mb ageostrophic wind for 1200 GMT on day C is partitioned into its tangential and normal components. For the ND sample there is no apparent pattern for either component. However, for D and JS definite patterns emerge. For example, note that the tangential components (Figs. 9c,e) clearly reflect the curvature of the streamlines shown in Figs. 7c,e. West of the inflection points of the streamlines, the tangential ageostrophic components point backward (toward the southwest and west), indicating the subgeostrophic nature of flow in the trough. To the east of the inflection points, they point forward (toward the northeast and east) indicating supergeostrophic flow in the mean ridge. This illustrates the dominance of the curvature term of equation (1) in determining the tangential component of the ageostrophic wind.

The normal components of the 300 mb ageostrophic wind displayed in Fig. 9d,f reflect the dominance of the downstream acceleration term of equation (1). In both the D and JS samples the normal component vectors point toward the right of the flow over the Colorado and southern Great Plains area. As shown previously in Figs. 7c,e, this is in the exit region of the 300 mb jet streak and is consistent with the existence of the upper branch of the transverse indirect circulation in this area. Comparison of these components with those shown in the schematic illustration of a jet streak in Fig. 8.11 in Palmén and Newton (1969) support the concept of a transverse indirect circulation. Also, note in Figs. 9d,f that in the far southwestern United States the normal components of the 300 mb ageostrophic wind are directed toward the left of the flow (i.e., toward the north). This is consistent with the upper branch of a direct circulation in the entrance region of the jet streak. However, some of the very large ageostrophic values may reflect boundary problems in applying the Barnes technque in this region. Although the 300 mb ageostrophic components are displayed only for 1200 GMT of day C, the patterns for the other time periods are similar; however, they propagate along with the 300 mb wind maxima. The exception was on day C+1, especially 1200 GMT, when the pattern was less obvious. This is likely due to the various paths followed by the cyclones (and jet streaks) as the systems moved away from the cyclogenetic region in eastern Colorado from which the 39 cases were chosen. The more diffuse sea level pressure pattern on day C+1 also reflects this tendency (see Fig. 4).

The normal and tangential ageostrophic wind components at 850 mb cannot be easily related to the speed advection and curvature terms in equation (1) for two primary reasons. First, as noted in the diadic product calculations in (2) above, the isallohypsic term is of much greater importance at 850 mb than at 300 mb, and

Fig. 9. Tangential and normal components of the 300 mb ageostrophic wind for 1200 GMT, day C. a) tangential for ND, b) normal for ND c) tangential for D, d) normal for D, e) tangential for JS, f) normal for JS.

Fig. 10. Total ageostrophic wind at 850 mb

a) ND for 0000 GMT, day C; b) ND for 1200 GMT, day C ;

c) ND for 0000 GMT, day C+1; d) D for 0000 GMT, day C ;

e) D for 1200 GMT, day C; f) D for 0000 GMT, day C+1 ;

g) JS for 0000 GMT, day C ; h) JS for 1200 GMT, day C ;

i) JS for 0000 GMT, day C+1.

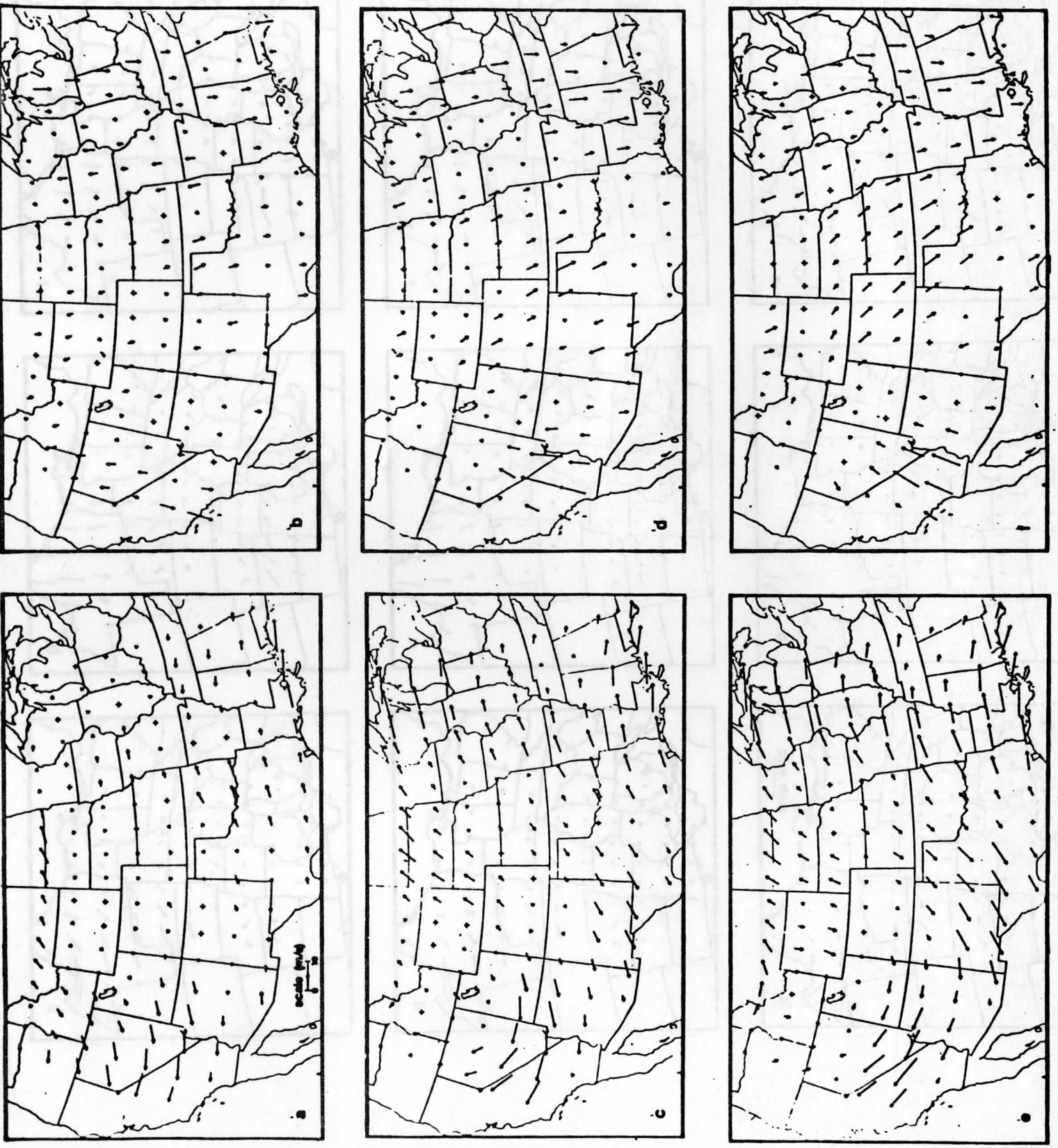

Fig. 9

Fig. 10

second, the frictional term in (1) can at times be significant at 850 mb, especially at 0000 GMT. Consequently, only the total 850 mb ageostrophic wind vectors are presented in Fig. 10 for 1200 GMT on day C-1 and both periods (0000 and 1200 GMT) on day C. A marked diurnal tendency in the ageostrophic wind is particularly notable in the Southern Great Plains. At the 0000 GMT hour the ageostrophic wind has a relatively large easterly component in this region, while at the bracketing 1200 GMT hours there is a strong southerly component. At this time the nocturnal stability tends to decouple the 850 mb winds from the surface flow, thus enhancing the relative significance of the isallohypsic term. Note the larger ageostrophic values in the D and JS samples, (especially the JS sample) than in the ND sample. Also, the largest 24h height falls, in excess of -60 m at 850 mb, were centered over extreme northeastern Kansas, which agrees well with the ageostrophic mass divergence associated with the upper branch of the indirect circulation. Finally, the presence of large southerly ageostrophic components in this region suggest that they are associated with the lower branch of the transverse indirect circulation in the exit region of the jet.

5. Conclusions

While the selection of events used in this study was done by Hovanec and Horn (1975) simply on the basis of spring season cyclogenetic occurrences, the results achieved here reveal that the composite of those cases which led to significant cyclone development (i.e., the D sample which includes the JS sample) are characterized by the presence of a clearly defined 300 mb jet streak propagating into the Southern Plains and the development of an 850 mb southerly wind maximum. In contrast, the composite of the cyclogenetic events which failed to develop (ND) lacked both a 300 mb jet streak and a LLJ.

Analyses of the observed 300 and 850 mb wind fields reveal isotach and streamline patterns which are consistent with the existence of a transverse indirect circulation in the exit region of the jet streak. In the developing case sample (D) and the JS subsample selected from it, the 850 mb southerly wind maxima (LLJ) is located directly beneath the exit region of the upper tropospheric jet. While this relationship is clear in the D sample, it is enhanced in the JS sample. A definite diurnal pattern is superimposed on the 850 mb winds with the nocturnal winds being considerably stronger and exhibiting an inertial oscillation tendency.

To more completely investigate the relationship between the 300 and 850 mb flows, ageostrophic winds were calculated at both levels. An examination of

the effects which contribute to the 300 mb ageostrophic winds indicated that the tangential components clearly reflect the effects of curvature in the flow and that the normal components primarily result from alongstream accelerations. In the exit region of the mean 300 mb jet these normal components apparently represent the upper branch of the transverse indirect circulation found in this region. At 850 mb the total ageostrophic wind values, especially at night, appear to be a response to 850 mb height falls which occur as mass at higher elevations (e.g., 300 mb) moves from the left to the right side of the propagating jet streak. This appears to further confirm that the upper and lower tropospheric jets are coupled through an indirect circulation in the exit region.

While an upper tropospheric polar jet and a LLJ have long been recognized as important components of the synoptic pattern associated with Colorado cyclones and outbreaks of severe weather, the two jets have usually been treated as separate phenomena. The results achieved here, using a composite approach rather than a series of individual case studies, provide support for the Uccellini and Johnson (1979) and Uccellini (1980) contention of their coupling. In Part II of the study which follows, Marshment and Horn (1981) use the same data sample and composite approach to examine moisture distribution and its role in destabilizing the atmosphere in these severe weather producing synoptic situations.

Although this paper has not employed satellite data, the information gained can aid the forecaster who uses satellite soundings to monitor the upper tropospheric jet in the Central United States. Once the thermal support of the upper jet is located, the results of this study can be used as a "model" of the location and evolution of the important LLJ; a feature which cannot be directly monitored by satellite soundings.

Acknowledgements

The assistance of Dr. Thomas Koehler in making suggestions involving the design of the study and providing programming aid was especially helpful. We also thank him for his comments regarding the manuscript. Thanks are also extended to Bob Lindmeir, Mary Hansen Bliesner and Pat Marvin for assisting with the data collection and to Brian Jarvis in drafting figures. The help of Kathi Marvin with the preparation of the final manuscript and Eva Singer in its typing is gratefully acknowledged. This research was supported by NOAA Grant NA 79AA-H-00011.

REFERENCES

Barnes, S.L., 1964: A technique for maximizing details in numerical weather map analysis. J. Appl. Meteor., 3, 369-409.

Beebe, R.G., and F.C. Bates, 1955: A mechanism for assisting in the release of convective instability. Mon. Wea. Rev., 83, 1-10.

Blackadar, A.K., 1957: Boundary layer wind maxima and their significance for the growth of nocturnal inversions. Bull. Amer. Meteor. Soc., 38, 283-290.

Bonner, W.D., 1968: Climatology of the low level jet. Mon. Wea. Rev., 96, 833-850.

Cahir, J.J., 1971: Implications of circulations in the vicinity of jet streaks at subsynoptic scales. Ph. D. Thesis, Penn. State Univ., 170 pp.

Fawbush, E.J., and R.C. Miller, 1953: The tornado situation of 17 March 1951. Bull. Amer. Meteor. Soc., 34, 139-145.

Fawbush, E.J., and R.C. Miller, 1954: The types of air masses in which North American tornadoes form. Bull. Amer. Meteor. Soc., 35, 154-165.

Hovanec, R.D., and L.H. Horn, 1975: Static stability and the 300 mb isotach field in the Colorado cyclogenetic area. Mon. Wea. Rev., 103, 628-638.

Lettau, H.H., 1967: Small to large scale features of boundary structures over mountain slopes. Proc. Symp. on Mountain Meteor., (ed. E.R. Reiter), Col. State Univ., 1-74.

Marshment, R.A., and L.H. Horn, 1981: Spring season cyclogenesis. Part II: Distribution of atmospheric water vapor and its influence on Static Stability. Mon. Wea. Rev., ___, _____.

Means, L.L., 1952: On thunderstorm forecasting in the central United States. Mon. Wea. Rev., 80, 165-189.

_____, 1954: A study of the mean southerly wind maximum in low levels associated with a period of summer precipitation in the middle west. Bull. Amer. Meteor. Soc., 35, 166-170.

Murray, R., and S.M. Daniels, 1953: Transverse flow at entrance and exit to jet streams. Quart. J.R. Meteor. Soc., 79, 236-241.

Newton, C.W., 1967: Severe convective storms. Advances in Geophysics. Vol. 12, Academic Press, 257-303.

Palmén, E., and C.W. Newton, 1969: Atmospheric Circulation Systems. Academic Press, 316-326.

Reiter, E.R., 1963: Jet-Stream Meteorology, The Univ. of Chicago Press, Chapt. 4 and 6.

Uccellini, L.W., 1980: On the role of upper tropospheric jet streaks and leeside cyclogenesis in the development of low-level jets in the Great Plains. Mon. Wea. Rev., 108, 1689-1696.

Uccellini, L.W., and D.R. Johnson, 1979: The coupling of upper and lower tropospheric jet streaks and implications for the development of severe convective storms. Mon. Wea. Rev., 107, 682-703.

Whittaker, T.M., 1977: Automated streamline analysis. Mon. Wea. Rev., 105, 786-788.

Spring Season Colorado Cyclogenesis. Part II: Distribution of Atmospheric Water Vapor and its Influence on Static Stability

Roberta A. Marshment* and Lyle H. Horn

Abstract

In Part I Achtor and Horn (1981) used a composite of 39 cases of April and May Colorado cyclogenesis to examine the relationship between the 300 mb jet streak and 850 mb southerly flow. In Part II the same set of days is used to study the moisture distribution and its influence on static stability. A composite approach is employed to prepare maps showing the moisture distribution at the surface and also at 900, 850 and 700 mbs. Data from the day preceding and the day following cyclogenesis are used to reveal the evolution of the moisture and static stability fields. Cross sections are constructed to show the vertical extent of the moisture and also the diurnal variation of the wind which transports the moisture northward.

In the composite a narrow tongue of moisture extends northward on the day preceding cyclogenesis. This tongue expands and shifts eastward on the following two days. The moisture is mainly confined to the layer below 850 mb, resulting in a tendency for potential instability. The cross sections not only confirm the concentration of moisture at low elevations, but also reveal stronger southerly flow at 1200 GMT than at 0000 GMT. The strongest southerly winds and maximum northward moisture transport occur under the exit region of the 300 mb jet streak. Maps of the Showalter index show the weakest static stability directly beneath the exit region of the jet streak, with the largest 24 hour decrease in static stability located to the east. As the 300 mb jet streak propagates into the central United States, the area of maximum decrease in the Showalter index shifts rapidly eastward.

*Present Affiliation
Meteorologist
WISC-TV, Madison, WI 53711

1. Introduction

In Part I Achtor and Horn (1981) used a data sample consisting of days on which spring season Colorado cyclogenesis occurred to study the relationship between the upper tropospheric westerly jet streak and the low level southerly jet. In this paper (Part II) we use the same sample of days to examine the moisture distribution and its influence on static stability during Colorado cyclone events.

The Gulf of Mexico is the primary source of moisture for Colorado cyclones. This moisture is not only the major source of precipitation in the central United States, but its horizontal and vertical distributions are of major significance to outbreaks of severe local weather, particularly during the spring season. The low level jet, which frequently lies beneath the exit region of the upper tropospheric jet and in advance of the surface low pressure center, often carries a tongue of moisture rapidly northward. See the figure from Newton (1967) which is reproduced as Fig. 1 in Part I. Because the tongue of moisture is relatively shallow, it favors potential instability. Outbreaks of severe weather are common along the western edge of the moist tongue, which is frequently marked by a distinct dry line (Rhea, 1966).

In examining the moisture we shall use a composite approach similar to that used in Part I. Means of the moisture and static stability will be formed from days on which Colorado cyclogenesis occurred. In some cases the means for the preceding and following day will also be calculated. While the use of means smooths the dramatic features found in individual case studies, the use of a composite has distinct advantages as noted in Part I. The composite is likely to reveal the characteristics of the moisture and static stability which Colorado cyclones share in common.

2. Data sample and procedures

As noted in Part I, the original sample of cyclogenetic days was gathered by Hovanec and Horn (1975). A developing cyclone was defined as one in which one closed isobar was maintained for at least 72 hours (see Part I for more details).

Of the 71 cases of Colorado cyclogenesis during April and May 1964-1971, only the 39 developing cases form the composite used here.

Surface dew point means were calculated using surface data from both radiosonde and six-hourly reporting stations. The mean specific humidity was calculated from radiosonde data for the surface, 900, 850, and 700mb levels. In order to assess the role of moisture on static stability, both dry and moist static stability indices were calculated. The dry index was obtained by calculating the 700-300mb temperature difference, while the moist index used 850 and 500 mb temperature and humidity data to form the Showalter index. (The Showalter index is obtained by lifting an air parcel at 850 mb dry adiabatically to saturation and then moist adiabatically to 500 mb; the index is the temperature of the parcel subtracted from its 500 mb environment.) To provide a more complete picture of the vertical distribution and northward transport of moisture, cross sections were also constructed. Although the majority of the figures displayed in this paper are for 1200 GMT, cross sections were prepared for both 1200 GMT and 0000 GMT time periods to reveal the significant diurnal variation in the moisture transport.

3. Moisture distribution

The discussion of moisture distribution during Colorado cyclogenesis begins with a comparison of that distribution with the climatic mean. Fig. 1, adapted from Dodd (1965), shows the average surface dew point distribution for April and May combined. Maximum dew points are found along the Gulf of Mexico with a moderate decrease northward through the central United States and a sharper decrease westward across central and western Texas.

The departures of surface dew point temperatures for the cyclogenetic composite from the climatic mean are shown in Fig. 2. On the day preceding cyclogenesis (C-1) positive departures cover most of Texas, except the extreme west and panhandle, with a narrow moist tongue extending northward into Southern Nebraska (Fig. 2a). The negative departures over the eastern portions of central United States likely result from the dry air associated with anticyclones which precede Colorado cyclones, while the negative departures over west Texas probably result from the advection of dry air from the Southwest.

On day C (Fig. 2b) the tongue of moisture has greatly expanded, reaching northward to the Iowa-Missouri border and eastward through most of Mississippi. The strengthened gradient over western Texas likely results from an increased advection of dry air from the West. Subsidence commonly occurs in this region as

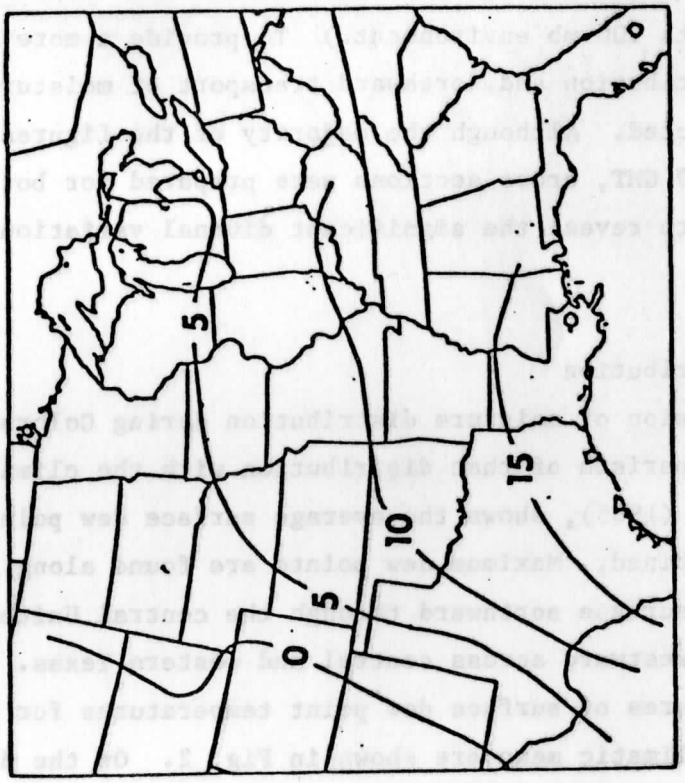

Fig. 1. Mean surface dew point distribution for April and May, combined. Adapted from Dodd (1965).

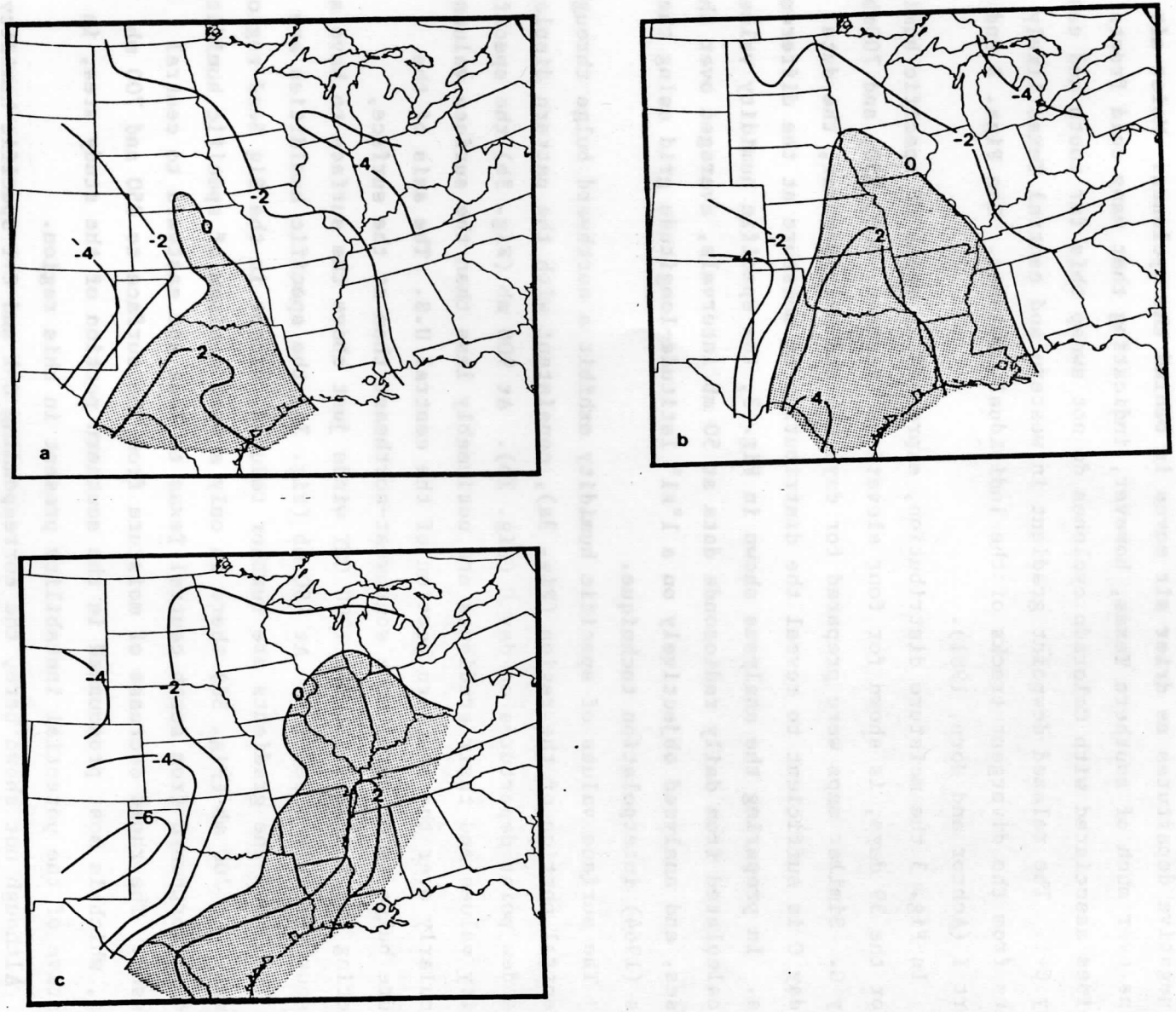

Fig. 2. Departure of 1200 GMT surface dew points (calculated for the 39 Colorado cyclogenesis cases) from the April and May mean shown in Fig. 1 for: a) day C-1, b) day C, c) day C+1. Positive values indicate that the cyclone sample values were larger than the April-May mean.

Colorado cyclones develop and probably contributes to the dryness in West Texas, which results in a strengthened moisture gradient.

On the day following cyclogenesis (C+1) the positive departures of dew points shift eastward as moist Gulf air flows northward ahead of the cyclone (Fig. 2c). Much of the central and western portions of the depicted region now have negative departures as drier air moves in behind the cyclones. Moist air remains over much of southern Texas, however, indicating that many cold fronts and dry lines associated with Colorado cyclones do not sweep this far south and east. by day C+1. The relaxed dewpoint gradient in western and central Texas likely results from the divergent tracks of the individual cyclones. See Figs. 3 and 4 in Part I (Achtor and Horn, 1981).

In Fig. 3 the moisture distribution, expressed as means of specific humidity for the 39 days, is shown for four elevations (surface, 900, 850, and 700mb) on day C. Similar maps were prepared for days C-1 and C+1; however, the data from day C is sufficient to reveal the distribution of moisture at the different levels. In preparing the analyses shown in Fig. 3, the specific humidity values were calculated from daily radiosonde data at 50 mb intervals, averaged over the 39 cases, and analyzed objectively on a 1°x1° latitude-longitude grid using the Barnes (1964) interpolation technique.

The surface values of specific humidity exhibit a northward bulge through the central portion of the region (Fig. 3a), consistent with the pattern displayed by the dew point departures on day C (Fig. 2b). At 900 mb (Fig. 3b) the specific humidity values and their gradients are noticeably less than the surface values, particularly over the southern portion of the central U.S. The axis of the moisture bulge is oriented more southwest-northeast than at the surface, reflecting the tendency for the 1200 GMT winds just above the surface to have a more southwesterly direction. At 850 mb (Fig. 3c) the specific humidities are again less, and the gradients are further reduced, except in the Big Bend region of Texas. At 700 mb (Fig. 3d) there is only a weak maximum of specific humidity extending northward from south central Texas to Iowa and eastward to central Tennessee. The rapid decrease of moisture from the surface to 850 and 700 mb levels, which is most pronounced in the southern portion of the study area, is indicative of the potential instability present in this region.

Although not shown here, the corresponding C-1 and C+1 specific humidity maps have a few features worth noting. The distribution of the low level moisture

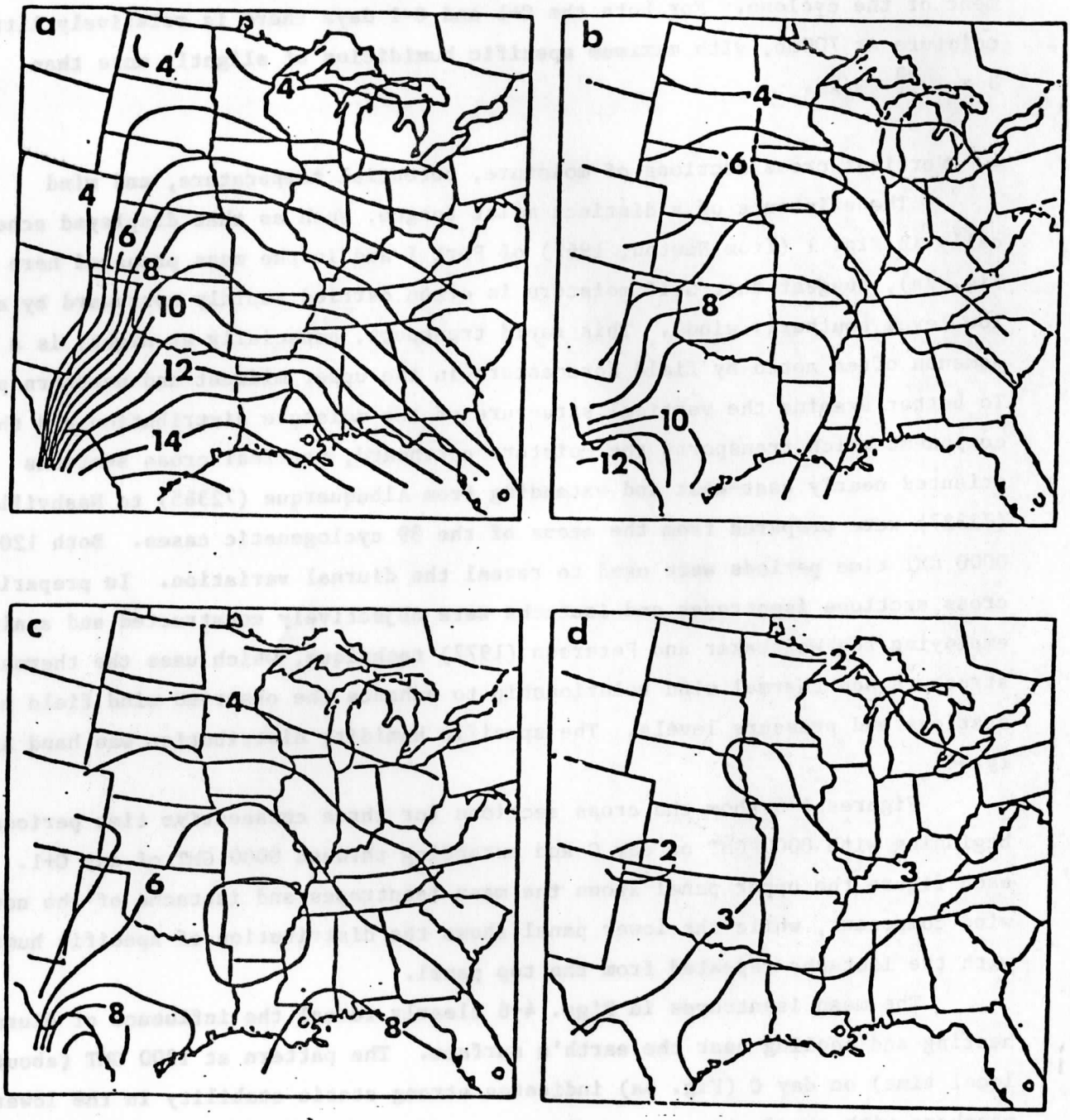

Fig. 3. Mean specific humidity (10^{-3}) on day C for a) surface, b) 900 mb, c) 850 mb, d) 700 mb.

through the time periods evolves in a manner similar to that shown in the dew point departure charts, moving first northward then eastward during the development of the cyclone. For both the C+1 and C-1 days there is relatively little moisture at 700mb, with maximum specific humidities of slightly more than 3×10^{-3} gm/kg.

4. Vertical cross sections of moisture, potential temperature, and wind

The existence of a distinct moist tongue, such as that displayed schematically in Fig. 1 (from Newton, 1967) of Part I and in the maps prepared here (e.g. Fig. 2a), suggest that Gulf moisture is often carried rapidly northward by strong low level southerly winds. This rapid transport, especially at night, is a phenomenon often noted by field forecasters in the upper midwest and northern plains. To better examine the vertical structure of the moisture distribution and the wind component which transports the moisture northward, vertical cross sections oriented nearly east-west and extending from Albuquerque (72365) to Nashville (72327) were prepared from the means of the 39 cyclogenetic cases. Both 1200 and 0000 GMT time periods were used to reveal the diurnal variation. In preparing the cross sections isentropes and isotachs were objectively constructed and analyzed employing the Whittaker and Petersen (1977) technique, which uses the thermal structure and thermal wind relationship to enhance the observed wind field between stations and pressure levels. The specific humidity distribution was hand analyzed.

Figures 4-6 show the cross sections for three consecutive time periods beginning with 0000 GMT on day C and extending through 0000 GMT of day C+1. In each figure the upper panel shows the mean isentropes and isotachs of the normal wind component, while the lower panel shows the distribution of specific humidity with the isotachs repeated from the top panel.

The mean isentropes in Figs. 4-6 clearly reveal the influence of diurnal heating and cooling near the earth's surface. The pattern at 1200 GMT (about dawn local time) on day C (Fig. 5a) indicates strong static stability in the lower troposphere with the isentropes running more-or-less parallel to the earth's surface. In contrast the isentropes for 0000 GMT (shortly before sunset local time) displayed in Figs. 4a and 6a show much weaker static stability, with some of the lower isentropes intersecting the surface at fairly large angles. The stronger static stability at 1200 GMTR on day C is also reflected in the greater wind shear between the surface and 900 mb.

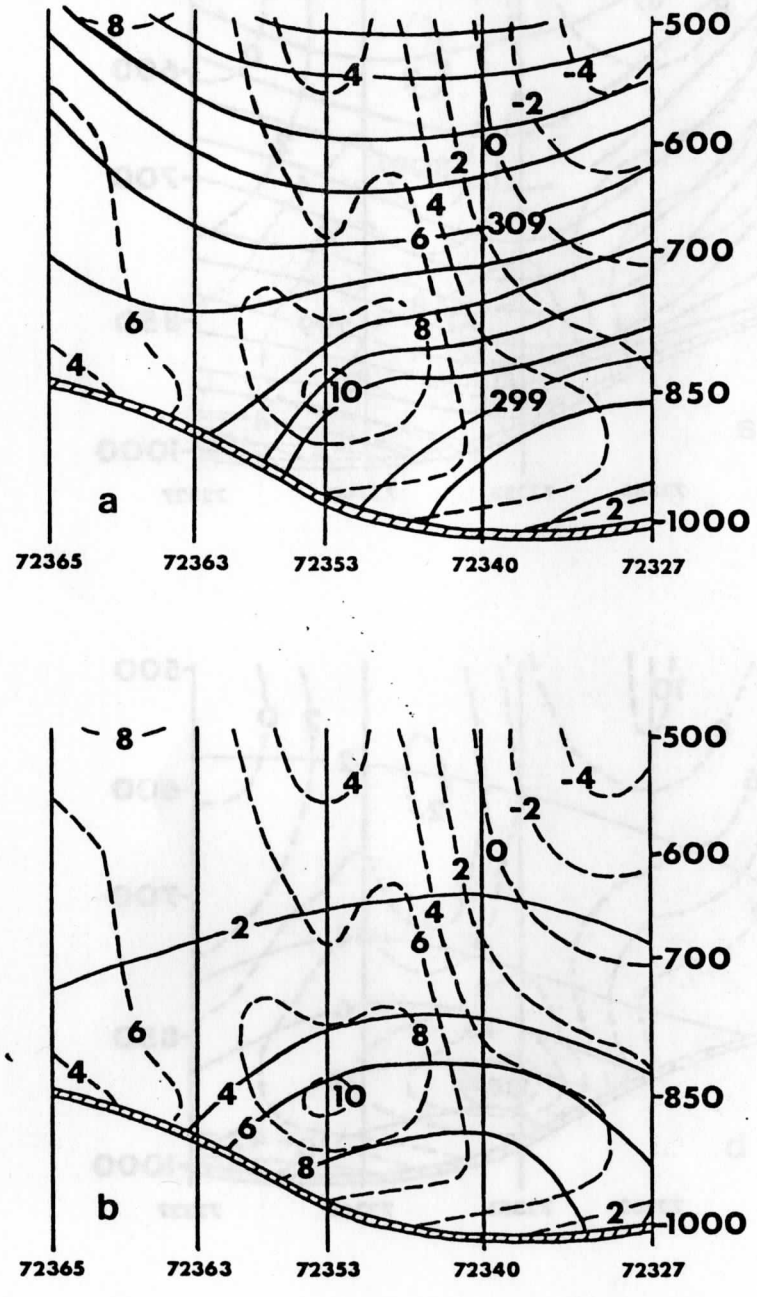

Fig. 4. Cross sections based on 39 day composite for 0000 GMT day C. a) Isentropes (solid lines) and isotachs of the normal wind component (dashed lines). b) Isolines (solid) of specific humidity (10^{-3}) with isotachs (dashed lines) repeated from top panel.

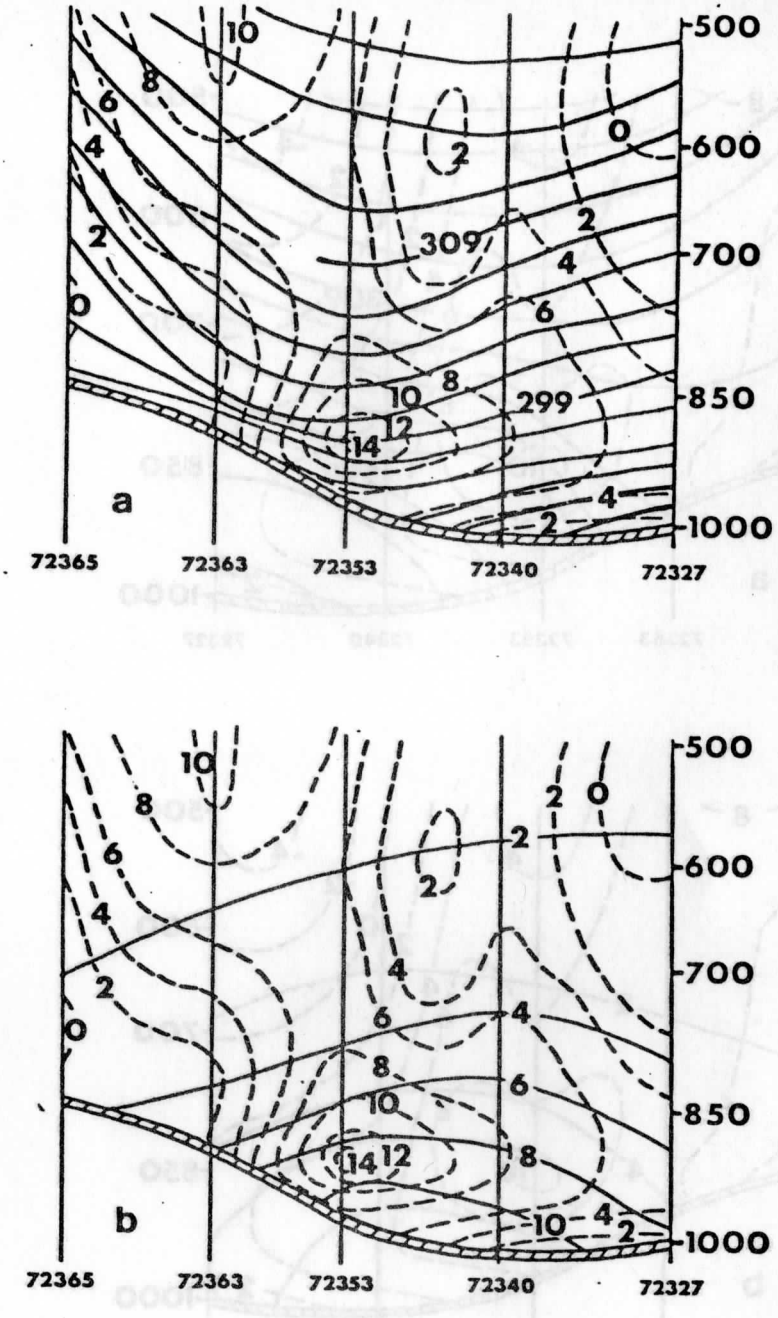

Fig. 5. Same as Fig. 4 except for 1200 GMT day C.

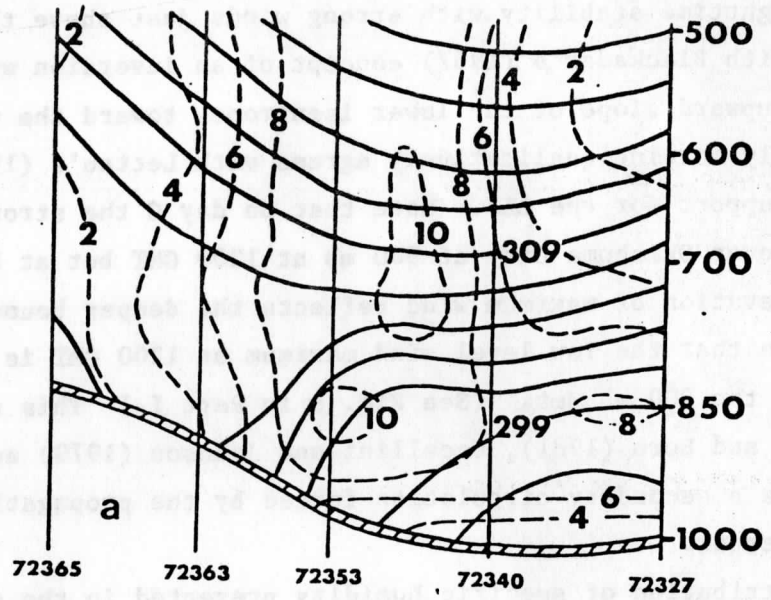

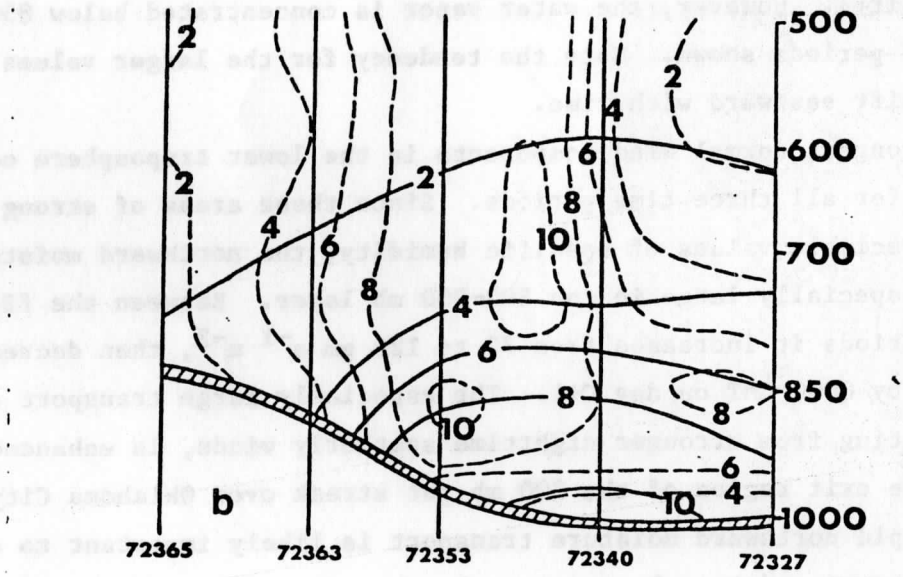

Fig. 6. Same as Fig. 4 except for 0000 GMT day C+1.

This nighttime stability with strong winds just above the stable layer is in agreement with Blackadar's (1957) concept of an inversion wind maximum. Moreover, the upward slope of the lower isentropes toward the west (colder air) during the early morning qualitatively agrees with Lettau's (1967) concept of thermal wind support for the LLJ. Note that on day C the strongest normal component occurs over Oklahoma City at 900 mb at 1200 GMT but at 850 mb at 0000 GMT. This higher elevation of maximum wind reflects the deeper boundary layer at 0000 GMT. Also note that the low level wind maximum at 1200 GMT is located under the exit region of the 300 mb jet. (See Fig. 8 in Part I.) This supports the contention by Achtor and Horn (1981), Uccellini and Johnson (1979) and Uccellini (1980) that the LLJ is a secondary circulation forced by the propagating upper troposphere jet streak.

The distribution of specific humidity presented in the cross-sections (Figs. 4b,5b,6b) shows an increase in the depth of the moist air from 0000 GMT of day C to 0000 GMT of day C+1 (e.g., note the positions of the 4 gm/kg isoline of specific humidity). However, the water vapor is concentrated below 850 mb during the three time periods shown. Note the tendency for the larger values of specific humidity to shift eastward with time.

The strongest normal wind components in the lower troposphere occur above Oklahoma City for all three time periods. Since these areas of strong winds coincide with appreciable values of specific humidity, the northward moisture transport is especially large in the 800-900 mb layer. Between the first and second time periods it increases from 70 to 126 gm s^{-1} m^{-2}, then decreases to 80 gm s^{-1} m^{-2} by 0000 GMT on day C+1. The especially large transport at 1200 GMT of day C resulting from stronger nighttime southerly winds, is enhanced by the presence of the exit region of the 300 mb jet streak over Oklahoma City at this time. This rapid northward moisture transport is likely important to continued cyclone development and to subsequent outbreaks of severe weather. The results shown in Figs. 4-6 suggest that the timing of the jet streak propagation into the Southern plains may be a significant factor in the northward moisture transport and thus in subsequent storm development.

5. Moisture and static stability

The mass-momentum adjustments in the exit region of a jet streak are thought to produce areas of reduced static stability (Uccellini (1977), Uccellini and Johnson (1979), Johnson and Sechrist (1970)). These adjustments can be adiabatic and do not require latent heat release. While the focus of this study

is on the influence of moisture, we also prepared a dry stability index consisting of the 700-300 mb temperature difference. The 700 mb level was chosen so as to be above any low level subsidence inversion. The static stability distribution described by this index can be compared with that obtained using the Showalter index, which is heavily dependent on moisture.

The results of the dry stability index are shown in Fig. 7. Larger values indicate weaker stability. On day C-1 the weakest stability revealed by the 700-300 mb temperature difference extends north-northwestward from south-central Texas through the high plains just east of the Rocky Mountains. (Fig. 7a). By day C the weakest stability remains over southern Texas, but the northward extension is now through the central plains (Fig. 7b). This pattern is very similar to the one obtained by Hovanec and Horn (1975), who used the 800-300 mb temperature difference to compute a stability index but for only this one time period (1200 GMT at day C). The pattern for day C+1 shows weak stability remaining over Texas but with a truncated northward extension (Fig. 7c). This somewhat confusing pattern may result from the variety of paths followed by the individual cyclones.

The moist stability index displayed in Fig. 8 is the Showalter index (smaller values indicate weaker stability). Since these values were formed from a mean of 39 days, care should be taken not to interpret the values as measures of the actual potential for severe weather as is done for individual days. However, the distribution and evolution of the values is of significance. To facilitate comparisons between the static stability patterns and the jet streak, a few 300 mb isotachs are included in each panel of Fig. 8.

On day C-1 (Fig. 8a) a pronounced tongue of weak moist static stability extends northeastward from south-central Texas into Oklahoma. This contrasts with the more northwestward orientation of the isolines of the dry static stability index shown in Fig. 7a. At this time the exit region of the 300 mb jet streak is located well to the west over New Mexico (Fig. 8a). The relative orientations of the isolines of the dry and moist static stabilities at this time may reflect the general geographical features of the area more than the influence of the approaching jet streak. The weak dry static stability, as noted above, more-or-less lies in the lee of the Rocky Mountains, which is common in this region. See Gates (1961) and Hovanec and Horn (1975). On the other hand, the orientation of the moist static stability isolines in this composite study may result from a tongue of Gulf of Mexico moisture moving around the western edge of the North Atlantic subtropical high, across northeastern Mexico, into south-central Texas in advance of the incipient cyclone.

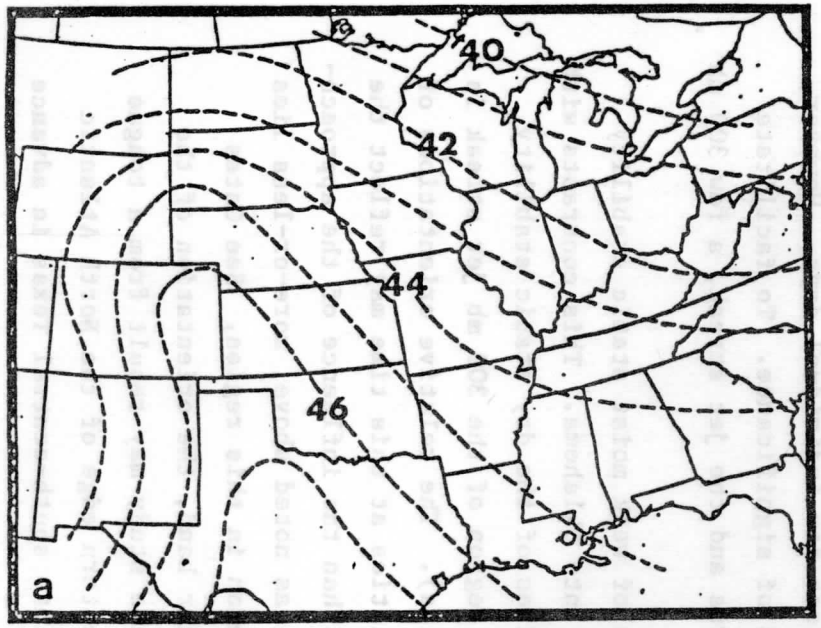

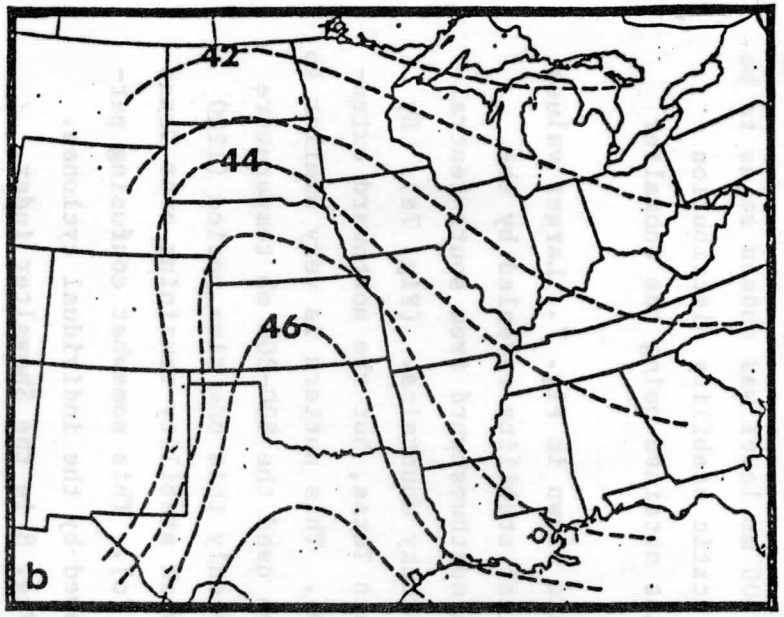

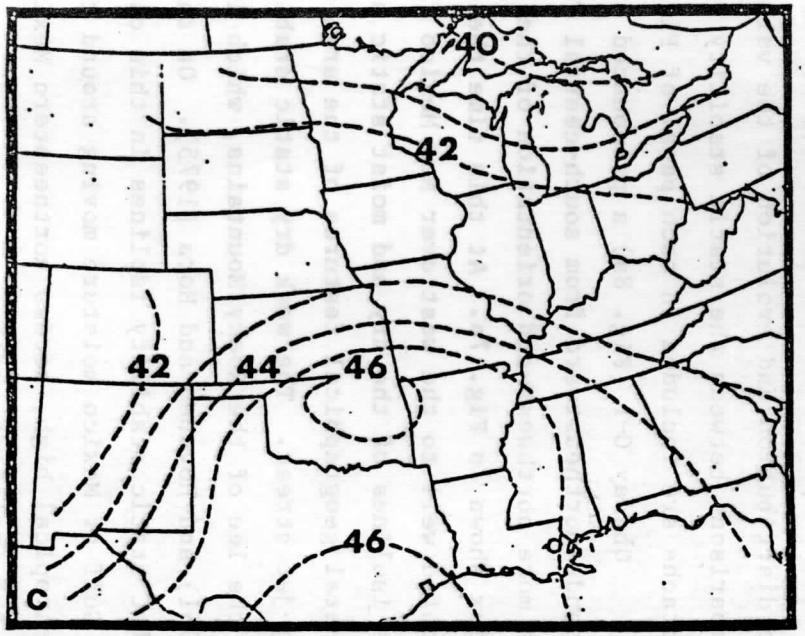

Fig. 7. Dry static stability as revealed by the 700-300 mb temperature difference (°C) at 1200 GMT for a) day C-1, b) day C, c) day C+1.

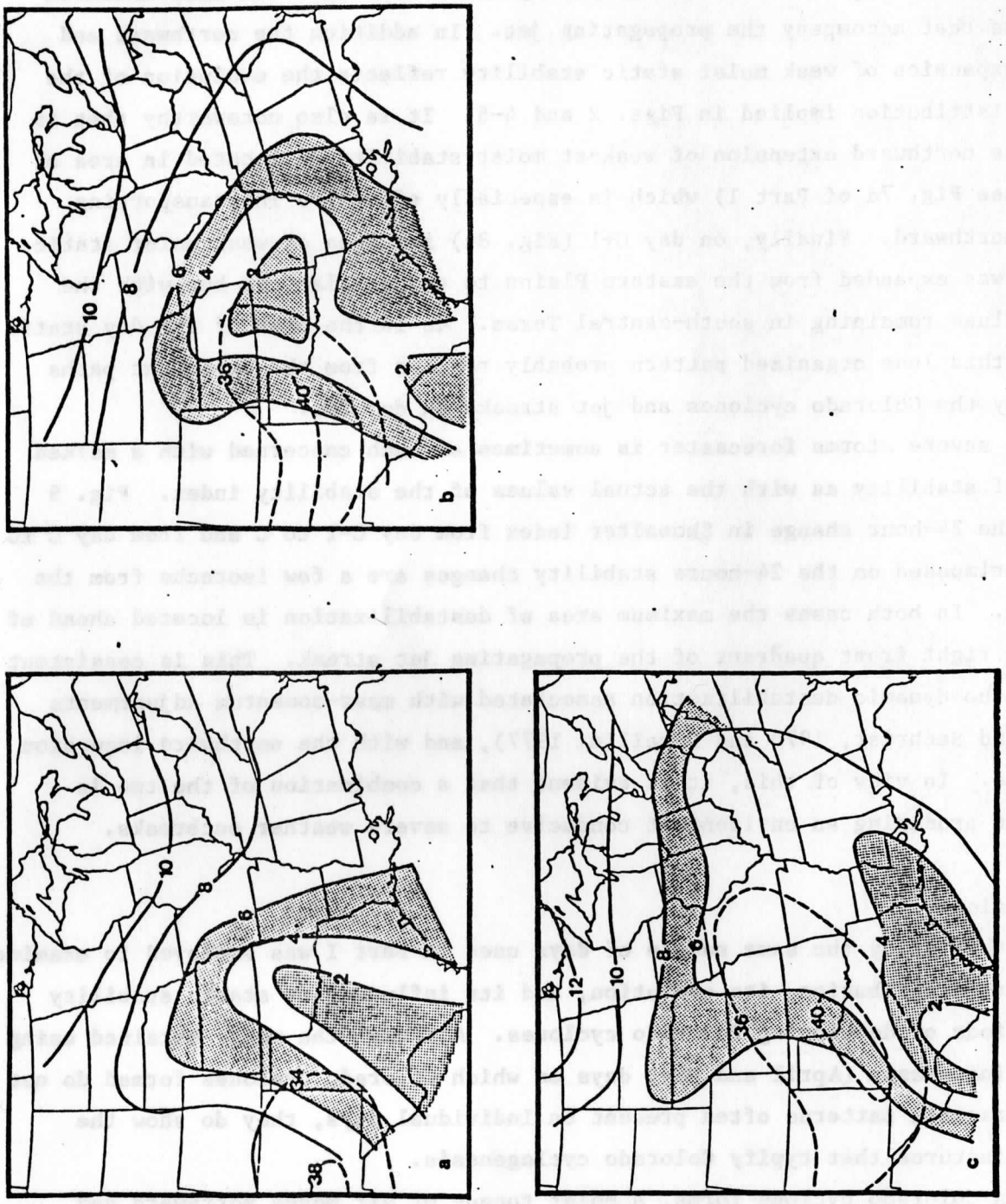

Fig. 8. Showalter index at 1200 GMT for a) day C-1, b) day C, c) day C+1 with a few 300 mb isotachs (dashed) superimposed.

By day C (Fig. 8b) the jet streak exit region has moved over the southern Plains with weak stability, found beneath it. A comparison of the isolines of dry (Fig. 7b) and moist static stability shows somewhat similar configurations, both likely resulting from the vertical stretching associated with the mass-momentum adjustments that accompany the propagating jet. In addition the northward and eastward expansion of weak moist static stability reflects the evolution of the moisture distribution implied in Figs. 2 and 4-6. It is also noteworthy that in Fig. 8b the northward extension of weakest moist stability is located in area of the LLJ (see Fig. 7d of Part 1) which is especially effective in transporting moisture northward. Finally, on day C+1 (Fig. 8c) the area of weak moist static stability was expanded from the eastern Plains to the Appalacians but with the minimum values remaining in south-central Texas. As in the case of the dry static stability this less organized pattern probably results from the divergent paths followed by the Colorado cyclones and jet streaks on day C+1.

The severe storms forecaster is sometimes as much concerned with a marked decrease of stability as with the actual values of the stability index. Fig. 9 displays the 24-hour change in Showalter index from day C-1 to C and from day C to C+1. Superimposed on the 24-hours stability changes are a few isotachs from the 300 mb jet. In both cases the maximum area of destabilization is located ahead of and in the right front quadrant of the propagating jet streak. This is consistent both with the dynamic destabilization associated with mass-momentum adjustments (Johnson and Sechrist, 1970 and Uccellini 1977), and with the northward incursion of moisture. In view of this, it is evident that a combination of the two is involved in producing an environment conducive to severe weather outbreaks.

6. Conclusions

In this study the same sample of days used in Part I was employed to examine the moisture distribution, its evolution, and its influence on static stability during periods of developing Colorado cyclones. Although the means obtained using the 39 spring season (April and May) days on which Colorado cyclones formed do not show the dramatic patterns often present on individual days, they do show the important features that typify Colorado cyclogenesis.

As a Colorado cyclone forms, a moist tongue of air moves northward and broadens. During this time a sharp gradient of moisture exists and remains in western Texas. Although the area of moisture expands eastward with the cyclone development, the vertical extent of the moist air shows only a minor increase. Thus potential instability is maintained in the region.

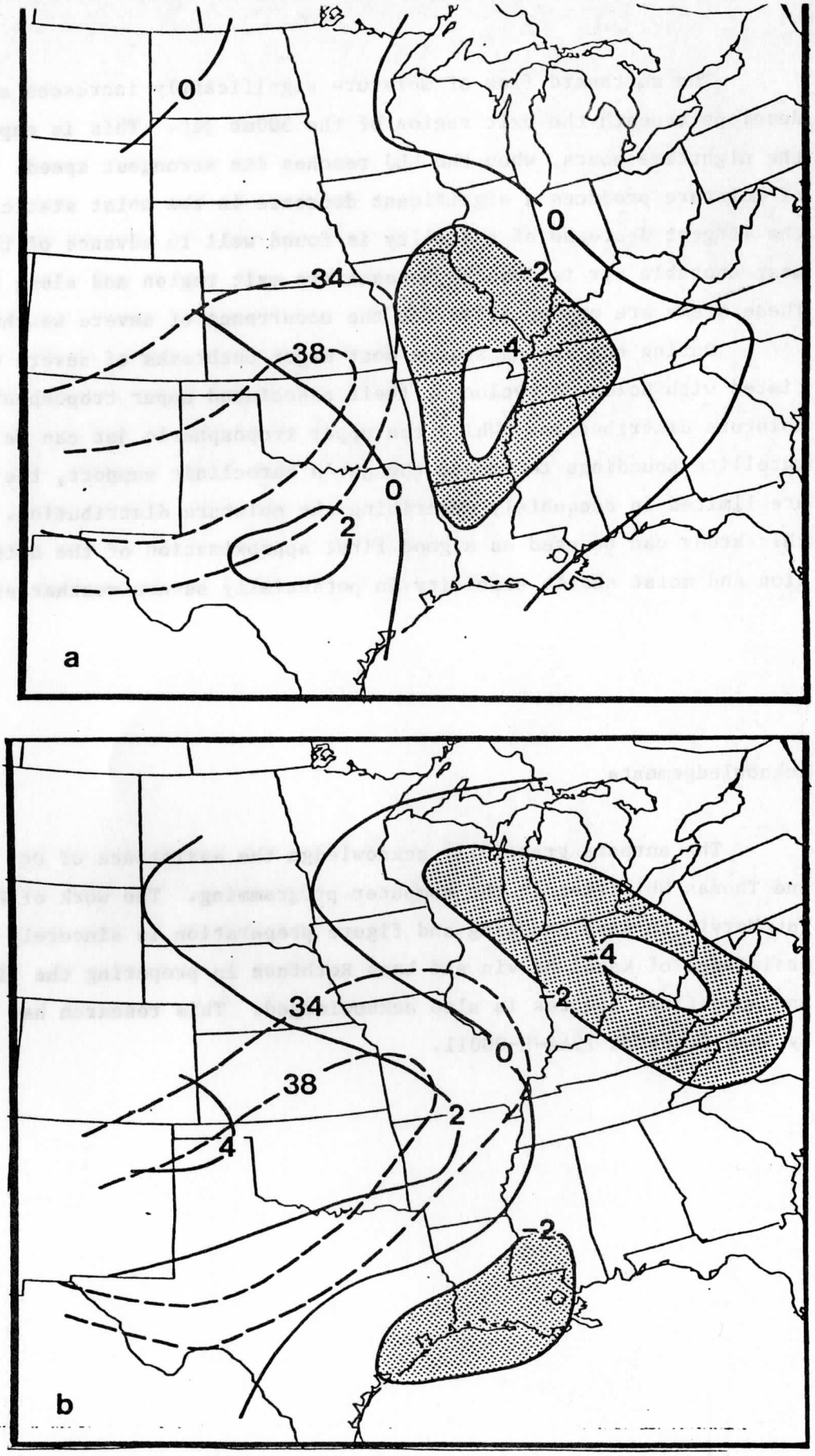

Fig. 9. Twenty-four hour change in 1200 GMT Showalter index (solid lines) with a few 300 mb isotachs (dashed lines) superimposed. a) Change from day C-1 to day C, isotachs from day C. b) Change from day C to day C+1, isotachs from day C+1.

The northward flow of moisture significantly increases as the low level jet develops beneath the exit region of the 300mb jet. This is especially true during the nighttime hours, when the LLJ reaches its strongest speed. The northward flow of moisture produces a significant decrease in the moist static stability. While the largest decrease of stability is found well in advance of the 300mb jet, the most unstable air is located beneath its exit region and along its right flank. These areas are common sites for the occurrence of severe weather.

During the spring season most major outbreaks of severe weather are associated with Colorado cyclones, their associated upper tropospheric jets and moisture distribution. While the upper tropospheric jet can be monitored using satellite soundings to locate the jet's baroclinic support, the satellite data are limited in adequately describing the moisture distribution. The results of this study can be used as a good first approximation of the moisture distribution and moist static stability in potentially severe weather situations.

Acknowledgements

The authors gratefully acknowledge the assistance of Dr. Thomas Koehler and Thomas Whittaker in the computer programming. The work of Pat Thorson and Pat Marvin in data handling and figure preparation is sincerely appreciated. The assistance of Kathi Marvin and Lans Rothfusz in preparing the final manuscript and some final figures is also acknowledged. This research has been supported by NOAA Grant NA 79AA-H-00011.

REFERENCES

Achtor, T.A., and L.H. Horn, 1981: Spring season cyclogenesis. Part I: Evidence of the coupling of the upper tropospheric jet streak to the low level jet. Mon. Wea. Rev. , .

Barnes, S.L., 1964: A technique for maximizing details in numerical weather map analysis. J. Appl. Meteor., 3, 369-409.

Blackadar, A.K., 1957: Boundary layer wind maxima and their significance for the growth of nocturnal inversions. Bull. Amer. Meteor. Soc., 38, 283-290.

Dodd, A.V., 1965: Dew point distribution in the contiguous United States. Mon. Wea. Rev., 93, 113-122.

Gates, W.L., 1961: Static stability measures in the atmosphere. J. Meteor., 18, 526-533.

Hovanec, R.D., and L.H. Horn, 1975: Static stability and the 300mb isotach field in the Colorado cyclogenetic area. Mon. Wea. Rev., 103, 628-638.

Johnson, D.R., and F. Sechrist, 1970: On the isentropic representation of storms, dynamic destabilization and squall line formation. Invited paper presented at 51st Annual Meeting, American Geophysical Union, April 1970, Washington, D.C. Abstract, EOS, Trans. Amer. Geophys. Union, 51, 294.

Lettau, H.H., 1967: Small to large scale features of boundary structures over mountain slopes. Proc. Symp. Mountain Meteor., Colorado State University, 1-74.

Newton, C.W., 1967: Severe convective storms. Advances in Geophysics, Vol. 12, Academic Press, 2157-303.

Rhea, J.O., 1966: A study of thunderstorm formation along dry lines. J. Appl. Meteor., 5, 58-63.

Uccellini, L.W., 1977: The coupling of upper and lower tropospheric jet streaks and implications for the development of severe convective storms. Ph. D. Thesis, Univ. of Wisc., 130 pp.

Uccellini, L.W., 1980: On the role of upper tropospheric jet streaks and leeside cyclogenesis in the development of low-level jets in the Great Plains. Mon. Wea. Rev., 108, 1689-1696.

Uccellini, L.W., and D.R. Johnson, 1979: The coupling of upper and lower tropospheric jet streaks and implications for the development of severe convective storms. Mon. Wea. Rev., 107, 682-703.

Whittaker, T.M., and R.A. Petersen, 1977: Objective cross-sectional analyses incorporating thermal enhancement of the observed wind. Mon. Wea. Rev., 105, 147-153.